Deformation bands in high-porosity sandstones: do they help or hinder CO2 migration and storage in geological formations?

Pourmalek, A., Newell, A., Shariatipour, S. M., Butcher, A., Milodowski, A., Bagheri, M. & Wood, A.

Original citation & hyperlink:
Pourmalek, A, Newell, A, Shariatipour, SM, Butcher , A, Milodowski, A, Bagheri, M & Wood, A 2021, 'Deformation bands in high-porosity sandstones: do they help or hinder CO2 migration and storage in geological formations?', International Journal of Greenhouse Gas Control, vol. 107, 103292.
https://dx.doi.org/10.1016/j.ijggc.2021.103292

DOI 10.1016/j.ijggc.2021.103292
ISSN 1750-5836

Publisher: Elsevier

Deformation bands in high-porosity sandstones: do they help or hinder CO_2 migration and storage in geological formations?

Azadeh Pourmalek[1], Andrew J. Newell[2], Seyed M. Shariatipour[1], Andrew S. Butcher[2], Antony E. Milodowski[3], Adrian M. Wood[4], Mohammadreza Bagheri[1]

Fluid and Complex Systems Research Centre, Faculty of Engineering, Environment and Computing, Coventry University, CV1 2NL

British Geological Survey, Maclean Building, Wallingford, OX10 8BB

British Geological Survey, Nottingham, United Kingdom, NG12 5GG

School of Energy, Construction and Environment, Coventry University, CV1 2LT

Keywords

Deformation Bands, Carbon Capture and Storage, Geological CO_2 Storage

Abstract

Small-scale deformation bands in Penrith Sandstone are used to assess the extent to which these features can act as effective mini-traps and contribute to secure CO_2 geological storage. A comprehensive set of simulation scenarios is applied to one conjugate set of deformation bands and also to clusters of deformation bands, to evaluate the effects of i) deformation band density; ii) the contrast in host rock/deformation band permeability; and iii) deformation band geometry, orientation and distribution on fluid movement and its significance for CO_2 storage capacity and security.

The findings of this study show that one conjugate set of deformation bands can improve CO_2 storage security, depending upon the plunge angle of the hinge. It has also been demonstrated that a high contrast in permeability (at least three orders of magnitude) is necessary for the CO_2 to be effectively trapped by the deformation bands.

It is shown that the highest number of bands observed and modelled for Penrith Sandstone outcrop, with three orders of magnitude permeability contrast, is a configuration that can contribute to the secure storage of CO_2 without causing an injectivity issue. This study shows that storage security is not only controlled by the contrast in permeability, but also by the permeability of the host rock. Furthermore, some geometries may contribute to storage security, while others may compromise it. To improve storage capacity and security for the type of reservoir studied herein, the results demonstrate the importance of accounting for the optimum injection rate and well placement.

1 **Introduction**

Permian and Triassic sandstone formations of continental aeolian origin are considered to be important target sites for the geological storage of CO_2 in the sedimentary basins of NW Europe (e.g., Permian Collyhurst Sandstone in the East Irish Sea Basin (Gamboa et al. 2019) and Permian Leman Sandstone of the Southern North Sea Basin (Holloway et al. 2006)). Aeolian sandstone formations offer good storage capacity as they are often thick and homogeneous, with good reservoir characteristics such as high porosity and permeability (Ringrose and Bentley 2015). However, it is also known fluid flow in such reservoirs can be impacted by faulting, in particular the formation of sand-to-sand fault seals along the deformation bands (e.g., Ogilvie et al. 2001; Van Hulten 2010; Ballas et al. 2015).

The literature describing the petrophysical properties of deformation bands in siliciclastic and carbonate rocks is quite extensive (Ballas et al. 2015 and references therein). Several authors have established how these structural features can have significant effects on subsurface flow in hydrocarbon reservoirs (Manzocchi et al. 1998; Rotevatn et al. 2008; Rotevatn and Fossen 2011; Fachri et al. 2013; Antonellini et al. 2014b; Zuluaga et al. 2016; Qu and Tveranger 2016; Rotevatn et al. 2017). However, despite the potential importance of high-porosity aeolian sandstones for CO_2 storage, the impact of deformation bands (especially the influence of conjugate deformation bands) on supercritical CO_2 injection and storage has been overlooked and has not been tested using flow simulation. To date, only one fluid flow experiment at sub-core scale, with the accompanying numerical simulations, has been undertaken on a core containing deformation bands in an attempt to determine the multiphase flow properties of these structural features in the CO_2 storage context (Romano et al. 2020). Thus at a reservoir scale, it is uncertain whether the reduction in effective reservoir permeability by deformation bands in otherwise high-quality reservoirs and aquifers will either adversely impact CO_2 injection and storage, or by creating a large number of mini structural traps, will enhance storage security at injection sites and reduce the reliance on maintaining the integrity of a single stratigraphic seal.

In response to this dearth of information, the main aim of this paper is to examine the impact of this commonly-developed structural configuration on geological CO_2 storage. To achieve this, static models were built that in a simplified way incorporated information on the structure and porosity-permeability characteristics of deformation bands from the Permian aeolian Penrith Sandstone Formation of NW England, as well as from the broader literature (e.g., Aydin et al. 1978; Torabi et al. 2008; Fossen et al. 2017), so that they could be imported into a flow simulator. The key questions addressed in the work include:

a) How does the geometrical architecture of the deformation bands influence storage security?
b) How does the deformation band density influence fluid communication and storage security?
c) How does the deformation band orientation, with regard to a major fault, affect storage security?
d) How might the permeability of the deformation bands, relative to the host rock, affect CO_2 storage effectiveness? How much permeability contrast is needed for deformation bands to trap CO_2 effectively?
e) Finally, and more importantly, do these sub-seismic reservoir heterogeneities have applications as structural traps?

1.1 Origins and characteristics of deformation bands

Rock failure in a porous granular material (φ >15%), such as sandstones and conglomerates (Aydin and Johnson 1983; Fisher and Knipe 2001; Aydin et al. 2006; Nicol et al. 2013; Fossen et al. 2017) or carbonate grainstones (Tondi et al. 2006; Antonellini et al. 2014a; 2014b; Rotevatn et al. 2017), can produce millimetre to centimetre-thick tabular-planar, low displacement deformation features, generally known as deformation bands (Aydin 1978). These structures can extend for tens or hundreds of metres (Aydin 1978; Antonellini and Aydin 1994; Fossen et al. 2007). The evolution of these structural discontinuities in porous sandstones typically follows three stages: formation of an individual deformation band; amalgamation of single deformation bands and the creation of a deformation band cluster;

and finally, the development of a slip plane within the deformation band cluster zone (Aydin 1978; Aydin and Johnson 1983; Antonellini and Aydin 1994). From an individual deformation band to the slip plane, an offset of a few millimetres to tens of metres is recognisable (Jamison and Stearns 1982; Aydin and Johnson 1983; Antonellini and Aydin 1994).

Deformation bands cannot be identified using seismic imaging (Fowles and Burley 1994; Walsh and Heath 1998) and can develop in non-tectonic and tectonic settings (extensional or contractional). In a contractional regime, deformation bands are widely and evenly distributed, whereas in an extensional regime, they are concentrated around major faults (Jamison and Stearns 1982; Fisher and Knipe 2001; Rotevatn et al. 2009; Solum et al. 2010; Rotevatn et al. 2013; Soliva et al. 2013; Schueller et al. 2013; Ballas et al. 2015; Zuluaga et al. 2016; Fossen et al. 2017).

The process of deformation in porous granular material is facilitated by the presence of pore space that allows for several deformation mechanisms, which are controlled by internal (host rock properties) and external factors (burial depth and stress state) (e.g., Fossen et al. 2007; Ballas et al. 2015). The main mechanisms involved in the formation of deformation bands are grain reorganisation (Twiss and Moores 1992; Du Bernard et al. 2002; Rawling and Goodwin 2003); cataclasis (Aydin 1978; Aydin and Johnson 1983; Underhill and Woodcock 1987; Du Du Bernard et al. 2002; Rawling and Goodwin 2003; Saillet and Wibberley 2010; Rotevatn and Fossen 2012; Fossen et al. 2015); phyllosilicate smearing (Antonellini and Aydin 1994; Fisher and Knipe 2001); and dissolution and cementation (Leveille et al. 1997; Tondi et al. 2006; Fossen et al. 2007). These mechanisms result in various types of deformation bands including disaggregation bands, phyllosilicate bands and cataclastic bands (see Fossen et al. 2007), with different petrophysical characteristics (e.g., porosity, permeability, and capillary entry pressure) that can impact fluid flow.

1.2 Effects of deformation bands on fluid flow

Deformation bands can act as both flow conduits and flow barriers. However, most observations have shown that deformation bands reduce porosity and permeability to some extent (Aydin 1978; Underhill and Woodcock 1987; Antonellini and Aydin 1994; Shipton et al. 2002; Rotevatn et al. 2008; Ballas et al. 2015). A permeability reduction depends on the type of deformation band. While disaggregation bands generally have little or no impact on the porosity and permeability, phyllosilicate bands (a sub-category of a disaggregation band), can reduce permeability by five orders of magnitude (Fisher and Knipe 2001). Cataclastic bands can in extreme cases result in a permeability reduction of up to six orders of magnitude (e.g., Underhill and Woodcock 1987; Antonellini and Aydin 1994; Fisher and Knipe 2001; Shipton et al. 2002), but more commonly two to four orders of magnitude relative to the host rock (e.g., Torabi et al. 2008). Deformation bands have a porosity of about one order of magnitude less than the surrounding host rock (Aydin and Johnson 1983; Antonellini and Aydin 1994; Torabi and Fossen 2009; Griffiths et al. 2018). In deformation bands where cataclasis is well-developed, capillary entry pressure measurements confirm the effective local sealing capacity of these structures with respect to a non-wetting phase (Antonellini and Aydin 1994; Torabi et al. 2013). Porosity, permeability (from zero to two or three orders of magnitude (Fossen et al. 2007; Torabi et al. 2008)) and thickness also vary along the bands (Rotevatn et al. 2013).

The effect of deformation bands on fluid flow dynamics and production performance has been addressed by various researchers using flow simulation (Matthäi et al. 1998; Olsson et al. 2004; Sternlof et al. 2006; Rotevatn and Fossen 2011; Rotevatn et al. 2013; Qu and

Tveranger 2016; Zuluaga et al. 2016; Qu et al. 2017; Rotevatn et al. 2017). These studies have shown that deformation bands in siliciclastic and carbonate reservoirs or aquifers are responsible for some flow-related phenomena including increased flow tortuosity, improved sweep efficiency, delayed water breakthrough and pressure compartmentalisation. The results demonstrate the importance of including damage zones (i.e., deformation bands) when investigating faulted high-porosity reservoirs.

Using flow simulations, Rotevatn et al. (2017) investigated the permeability and flow effects of individual deformation bands in porous carbonate rocks, concluding that deformation bands may have a greater influence than previously thought. In some lower permeability host rocks, they found that deformation bands seriously impeded flow when the permeability of the deformation bands was one-two orders of magnitude less than the low to the medium permeability host rock. This contradicts previous studies that showed deformation bands must have a large permeability contrast (three-four orders of magnitude) relative to the host rock to affect flow (e.g., Zuluaga et al. 2016). Also, many research studies have shown a positive effect of deformation bands on production (Rotevatn et al. 2009; Zuluaga et al. 2016; Fossen et al. 2017) while many others demonstrate their negative or negligible effects (Fossen and Bale 2007; Rotevatn et al. 2017). Moreover, it is not clear if they have a sealing capacity as suggested by Torabi et al. (2013), or, as Fossen et al. (2017) argued, these features do not tend to have sealing properties.

As previously indicated (Ringrose and Bentley 2015; Newell et al. 2019), gas reservoirs might only be sensitive to three orders of magnitude permeability contrast. Given the contradicting results and since it is not yet clear how much permeability contrast is necessary for the deformation bands to act as flow barriers, particularly in gas reservoirs, this study expands our knowledge on the effects of these structures in such reservoirs by considering broader, but still feasible, host rock permeability than previously applied (Rotevatn et al. 2009; Fachri et al. 2013; Zuluaga et al. 2016) and deformation bands permeability of Penrith Sandstone and many published data. When considering the role of deformation bands in CO_2 sequestration, this work also shows the importance of understanding their geometry, frequency, and location relative to larger structures.

2 Outcrop analogue example

2.1 Penrith Sandstone Formation of NW England

The Lower Permian Penrith Sandstone Formation of north-west England **(Fig. 1)** is a classic example of a high porosity aeolian sandstone in a rift basin setting that contains numerous deformation bands (Fowles and Burley 1994). The Penrith Sandstone Formation (abbreviated to Penrith Sandstone from here on) consists of up to 460 metres of aeolian cross-bedded sandstone (Lower Permian Rotliegend equivalent) contained within the fault-bounded Vale of Eden Basin. The succession unconformably overlies Carboniferous rocks and is overlain by mudstones and evaporites of the Upper Permian Eden Shales (Zechstein equivalent) and the Triassic St Bees Sandstone (Arthurton and Wadge 1981). The exposures described here are found within the Eden Gorge, close to their contact with the Eden Shales, which in a subsurface fluids context would form the topseal to the Penrith Sandstone reservoir **(Fig. 2).**

Data from the Penrith Sandstone is used here to guide the configuration of a static geological model so that the density, orientation, dimensions and permeability properties of deformation bands are within the boundaries of what might be expected for a given volume of aeolian sandstone. Information derived from the outcrop included, (1) direct field observations and measurements of deformation bands using scan-line surveys, (2) indirect mapping of structural and stratigraphic features on 3D base maps created by laser scanning outcrop cliff faces, and (3) analyse a representative set of field-collected samples of the Penrith Sandstone for porosity and permeability.

Figure 1: Map showing the location of the Eden field site in north-west England. Onshore and offshore distribution of Permo-Triassic outcrop based on Pharaoh et al. (1996). EISB = East Irish Sea Basin.

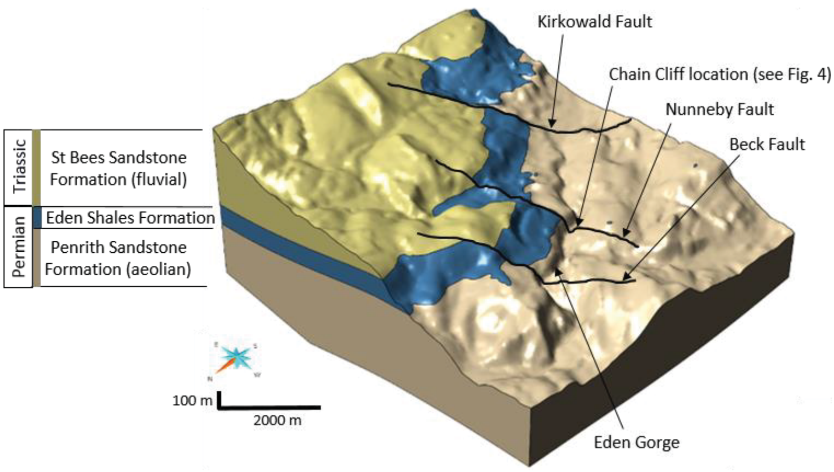

Figure 2: Block diagram showing local stratigraphy at the study site. Outcrops of the Penrith Sandstones are within the Eden Gorge just below the stratigraphic contact with the Eden

Shales. NE-SW trending faults which occur in association with the deformation bands are shown.

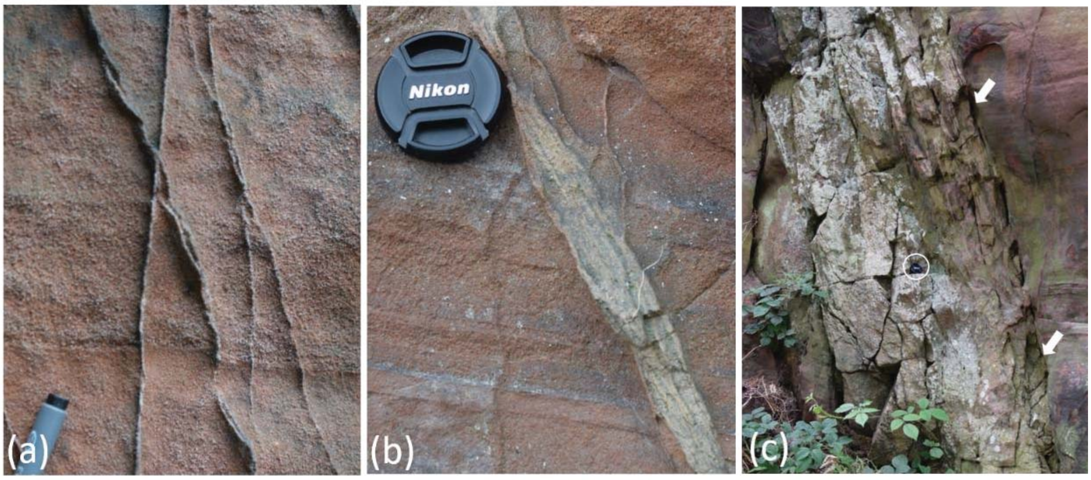

Figure 3: Variations in deformation band development from (a) Millimetre-wide bands showing conjugate cross-cutting arrangement, (b) Multiple anastomosing bands forming a zone several centimetres across, and (c) Thick zone composed of multiple bands with slip surface on the hanging wall (right hand) side. Note voids and fractures developed at releasing bends on the slip surface (arrows). Lens cap (circled) is for scale.

2.2 Petrographic and image analysis methods

Petrographic analysis was undertaken at the British Geological Survey (BGS) on 15 polished thin sections from a suite of 10 samples of sandstone containing intact deformation bands. Small (5-10 cm) samples were collected from cliff face outcrops of the Penrith Sandstone in the Eden Gorge near Lazonby (between National Grid Reference points NY 51894 44175 and NY 52135 43265) and near Armathwaite (National Grid Reference NY 50560 45174); and from a disused quarry near Cowraik (National Grid Reference NY 542 309). The samples were vacuum-impregnated in blue dyed epoxy-resin prior to thin sectioning, and the rock slices were mounted onto glass slides using colourless epoxy-resin. This enabled the blue epoxy-resin-filled porosity to be clearly differentiated during optical petrography from any grains that may have been plucked out (seen as colourless resin) during the sections’ polishing. The thin sections were cut perpendicular to the plane of the deformation bands and approximately perpendicular to the bedding. The thin sections were initially examined using a Zeiss Axioplan II optical petrographic microscope prior to more detailed back-scattered electron microscopy (BSEM) observations.

Scanning electron microscopy (SEM) was undertaken using a FEI QUANTA 600 environmental scanning electron microscope (ESEM). This was equipped with an Oxford Instruments INCA Energy 450 energy-dispersive X-ray microanalysis (EDXA) system with a 50 mm^2 Peltier-cooled (liquid nitrogen free) silicon drift detector (SSD); a solid-state backscattered electron (BSE) detector; and a Centaurus (Deben UK Ltd) parabolic mirror-type cathdoluminescence detector, providing monochromatic cathodoluminescence images (SEM-CL). The ESEM was operated in a conventional high vacuum mode. BSEM and EDXA analyses were performed with an electron beam accelerating voltage of 20 kV and a beam probe current of 34 pA, at a working distance of 10 mm. SEM-CL images were recorded using an electron beam accelerating voltage of 12.5 kV and a beam probe current of 0.22-0.24nA, at a working distance of 17 mm. Mineral/phase identification was aided by microchemical information obtained from simultaneous observations of semi-quantitative EDXA spectra, which were processed and interpreted using the Oxford Energy INCA Suite Version 4.15 Issue 18d+SP3 (2009) software package.

Wallrock porosity was determined by digital petrographic image analysis (PIA) of the BSEM images, using the FiJi (formerly ImageJ) (v.1.48k 15 December 2013) public-domain open-source software package (Rasband 2013). A sequence of overlapping BSEM images was recorded along profiles, across deformation bands and the adjacent host sandstone matrix (**e.g., Fig. 5a**). These were then “stitched” together to form a continuous mosaic image, using “Grid/Collection Stitching” plug-in macro in FiJi. The BSEM mosaic image “brightness” and “contrast” were adjusted to enhance the differentiation of porosity and then “thresholded”, so that the “grey-level” corresponding to the epoxy-resin-filled porosity was imaged as predominantly “black” pixels. The image was then “binarised” to produce a black and white image (**Fig. 5c**), and the percentage proportion of the image area occupied only by the “black” pixels (porosity) was digitally quantified.

2.3 Petrography of the undeformed Penrith Sandstone

The main dune-facies lithology of the Penrith Sandstone that hosts the deformation bands in the Eden Gorge is generally a well-sorted (cf. Fig.3.29, Stow 2005 (after Compton (1962)), medium- to coarse-grained sandstone (grain size predominantly 200-500 µm), but ranges from very fine to coarse sandstone (50-750 µm). The sand grains are predominantly subrounded to rounded, with common large well-rounded, millet-seed grains of up to 750 µm. Thin, finely horizontally-laminated, fine- to medium-grained interdune sandstones separate the thicker 1-3 m dune sandstones. The sandstones are quartz arenite to subfeldspathic arenite in composition (classification after Pettijohn et al. (1987)); dominated by major detrital quartz with between 5 to 20% detrital K feldspar. Both monocrystalline and polycrystalline detrital quartz are present. The sandstone also contains trace amounts of detrital iron oxides (magnetite and ilmenite), although no detrital organic particles are present.

The sandstones are close-packed, displaying predominantly simple point and concavo-convex grain contacts. They have been significantly modified by burial diagenesis and post uplift meteoric alteration (telodiagenesis).

The rocks are cemented by patchy, authigenic quartz developed as syntaxial overgrowths on detrital quartz, commonly with euhedral terminations into open pore space. Similarly, minor syntaxial authigenic overgrowths have formed on some of the detrital K-feldspar grains. These overgrowth cements have produced a rigidly “locked” grain fabric. Locally, horizons of very tough quartz-cemented sandstone are present in the sequence and are seen towards the top of the cliffs in the Eden Gorge and surrounding hilltops. These are impermeable and very tightly cemented by pore-filling authigenic quartz cement.

Although the sandstones are close-packed, large “oversized” intergranular pores (i.e., pores with similar or greater sizes than the grain size) are very common in the outcrop sandstones (e.g., **Fig. 5a and 5c**) and are typical of secondary porosity created by the dissolution of detrital framework grains (Schmidt and Mcdonald 1979a; 1979b). Relicts of quartz and traces of albite within these secondary pores indicate that the sandstones originally contained a higher proportion of feldspar (probably largely plagioclase) and possibly lithic grains. These have subsequently been lost through dissolution during burial diagenesis or later telodiagenesis. No evidence of carbonate cement was observed in the samples examined.

2.4 Deformation bands in Penrith Sandstone

On weathered surfaces, deformation bands in the Penrith Sandstone typically occur as seams of non-porous white sandstone standing out against a background of porous and undeformed red sandstone **(Fig. 3).** As recognised elsewhere (Aydin and Johnson 1983), the bands show a continuum of development from millimetre-wide seams which offset stratigraphic markers by a few millimetres, through to anastomosing clusters several centimetres thick and occasional zones of up to one metre thick, with slip surfaces developed along the margin **(Fig. 3).** The latter represents the development of through-going faults and is often associated with a high density of deformation bands in the immediate footwall and hanging wall of the fault **(Fig. 4).** The overall pattern is thus a complex network of X-shaped structural discontinuities with a highly variable density and development throughout the rock volume.

The lengths of the deformation bands are highly variable and difficult to determine in three dimensions because of the general lack of bedding-parallel exposures in the Eden Gorge. Using excavated caverns in the Penrith Sandstone, Seers and Hodgetts (2016) showed that individual deformation band segments are typically around 0.7 m in length, but these can combine to form zones of deformation bands that are often 1-10 m in length in a vertical direction and may extend for 15 m or more in the bedding parallel (horizontal) plane. BSEM observations of the thin sections of the deformation bands show the characteristic collapse of porosity, grain-size reduction and pervasive cementation relative to the undeformed sandstone matrix **(Fig. 5c)**. SEM-CL clearly reveals that the detrital grains of quartz and feldspar have been intensely fractured, crushed and comminuted **(Fig. 5b).** Many of the deformed sand grains show some degree of rotation of the fractured components. K-feldspar grains are typically more highly comminuted compared to quartz, probably because of their well-developed crystal cleavages. SEM-CL observations show that the deformation bands are tightly-cemented by a fine “matrix” of very finely comminuted detrital quartz (varying from brightly-luminescent to dull-luminescent quartz fragments) cemented by very dull- to non-luminescent authigenic quartz cement **(Fig. 5b)**. Non-luminescent and weakly-luminescent quartz cement also seal microfractures in the deformed detrital quartz grains.

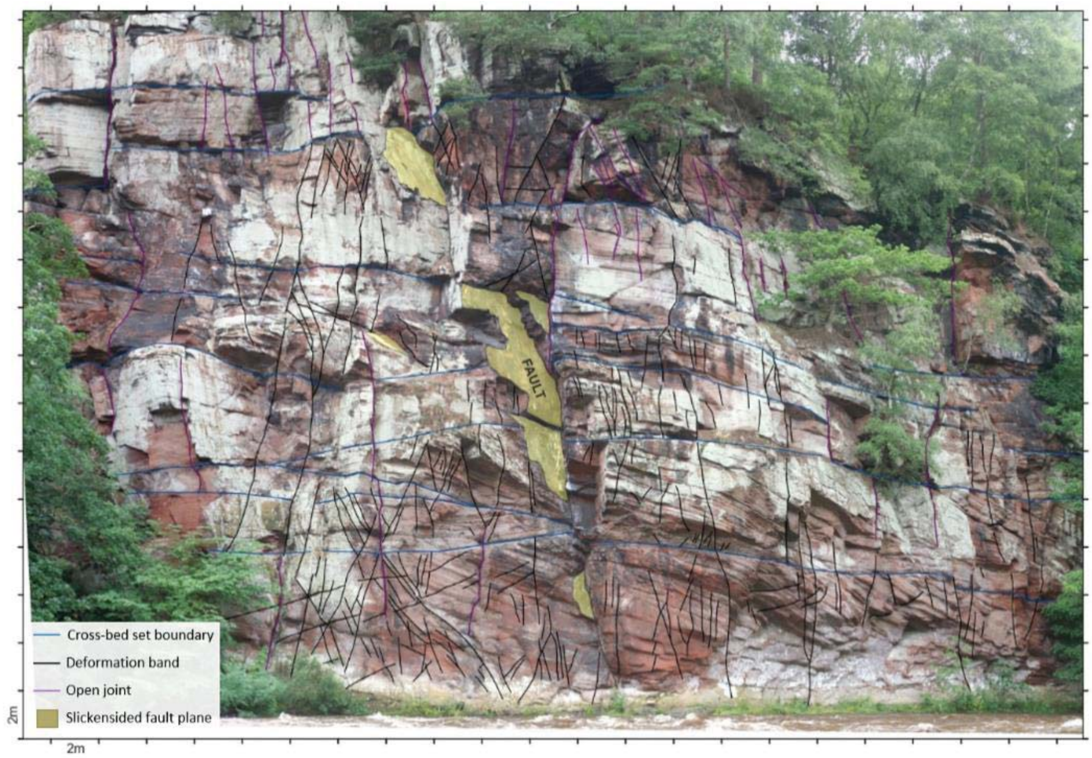

Figure 4: Map showing the distribution of deformation bands at Chain Cliff outcrop, Eden Gorge, where they are clustered around a fault plane. Deformation bands are shown in black, open joints are shown in purple and aeolian bedding surfaces are shown in blue. The outcrop is orientated 010-190° and the main fault plane (yellow colouration) dips at 80° toward 050°.

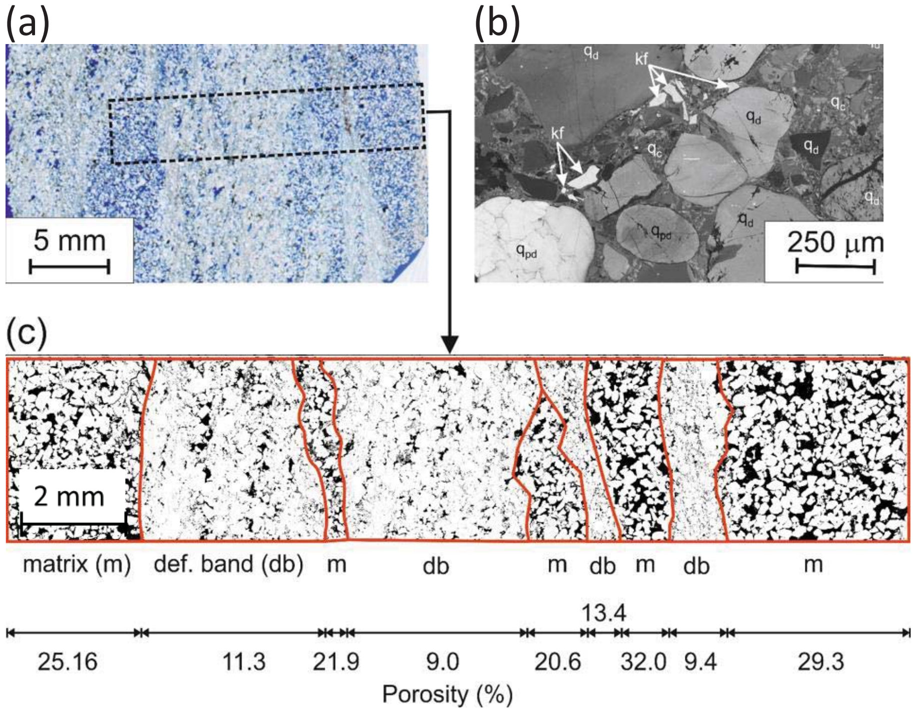

Figure 5: (a) Transmitted light image of highly porous blue-dyed resin-impregnated sandstone cut by a composite zone of anastomosing tightly-cemented, non-porous deformation bands (lacking blue-dyed resin impregnation). (b) SEM-CL image showing detail of the deformation fabric within a typical deformation band, with variably luminescent microfractured detrital monocrystalline (q_d) and polycrystalline (q_{pd}) quartz grains, fragmented brightly-luminescent detrital K-feldspar (K_f), within a tight "matrix" of highly comminuted detrital quartz fragments cemented by non- to very weakly-luminescent authigenic quartz cement (q_c). Non-luminescent quartz cement also fills microfractures in the quartz grains. (c) Thresholded and binarised composite BSEM mosaic showing the distribution of porosity (black). Total porosity values determined by image analysis, corresponding delineated domains of undeformed sandstone and deformation bands are shown.

2.5 Petrophysical properties of deformation bands and host rock

A representative set of field-collected samples of the Penrith Sandstone was analysed for porosity and permeability **(Fig. 6).** The samples included undeformed host sandstone (with various quantities of silica cement in the form of grain overgrowths) and sandstone containing deformation bands. Porosity was measured using the liquid resaturation method. Gas permeability tests were performed by steady-state methods on 2.5 cm diameter cylindrical plugs constrained in a core holder. Permeability was measured by establishing a constant flow rate of nitrogen through the sample. The results are in agreement with observations from many other studies (e.g., Torabi et al. 2008; Torabi and Fossen 2009; Torabi et al. 2013; Ballas et al. 2015; Fossen et al. 2017), which show that the presence of deformation bands can reduce sandstone permeability by several orders of magnitude.

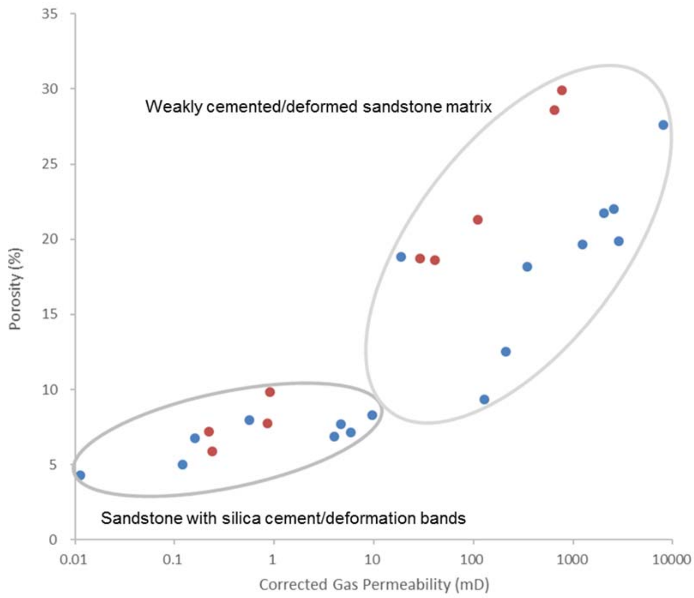

Figure 6: Porosity and permeability measurements from representative field-collected samples of the Penrith Sandstone. Blue points are core plugs (2.5 cm diameter) measurements based on liquid resaturation (porosity) and nitrogen gas permeability tests.

Red points are porosity estimated by the image analysis of polished thin sections and a predicted Carman-Kozeny permeability calculated from the total porosity and specific surface area. Both types of measurements show the existence of two broad fields corresponding to the host sandstone (porosity typically around 10-30 percent) and sandstone containing deformation bands with a porosity reduced to less than 10 percent and a permeability several orders of magnitude lower.

3 Methodology

A number of numerical simulations were conducted to investigate deformation bands in connection with CO_2 geological storage. The static models were generated in Schlumberger's Petrel software (Schlumberger 2016). Dynamic modelling studies were conducted using ECLIPSE 300 (Schlumberger 2017) with the CO2STORE module. For this study, the models were intentionally kept simple, with the incremental change of their parameters in order to isolate and evaluate the key factors governing flow movement in such reservoirs.

The framework for the geological models was comprised of the horizontal top surface and the horizontal base surface. No flow boundaries were considered for all sides of the models. Each model was uniformly gridded in the three main dimensions.

To generate a fracture/deformation bands network in Petrel, standard processes such as facies modelling and petrophysical modelling are conducted prior to fracture network modelling. It was assumed that the host rock was homogeneous throughout this study. In doing so, the effects of the deformation bands on the fluid flow were isolated.

To accurately calculate the contribution of the deformation bands to the fluid flow, a discrete fracture network (DFN) was used to explicitly populate the deformation bands in the reservoir models. This can be achieved using either a stochastic or a deterministic method. Certain observations must be input into the static models to model these structural heterogeneities stochastically, including the distribution and the extent of the deformation bands, the geometry of the deformation bands, their orientation and permeability. After assigning these properties, the associated deformation band surfaces can be imported to scale-up fracture network properties in Petrel, where the properties can be exported and used for flow simulation. The values used in this work are representative of the range found in Penrith Sandstone and in many published studies (e.g., Fisher and Knipe 2001; Torabi et al. 2008; Fossen et al. 2017).

In the first instance, the modelling considered the scenario of a single conjugate set of deformation bands (Section 4). The aim of this simple model setup was twofold. First to test the effect of varying the permeability contrast between the deformation bands and their sandstone matrix across three orders of magnitude. Second to examine the impact of changing the plunge angle of the hinge line between the two deformation bands. This research is important as it provides an idea of the flow at the scale of one conjugate set of bands, which helps to understand the flow at a reservoir scale. A simplified sandbox model with a spatial dimension of 20 m × 20 m × 20 m was developed and discretised into a total of one million active cells (ni=100, nj=100, nk=100) **(Fig. 7, Table 1**). Deformation bands were given a thickness of 2 cm, which was the minimum cell size at which the reservoir modelling software was still able to operate and the modelling was computationally feasible. In sandstone formations, deformation bands of this thickness can result from the amalgamation of multiple anastomosing seams (e.g., see **Fig. 3B**). The deformation bands were configured in the model as two mutually cross-cutting planes of opposing dip azimuth. The corresponding cells of these two surfaces were given the values of the deformation bands' porosity, permeability **(Table 3 and 4),** and flow properties **(Table 2).**

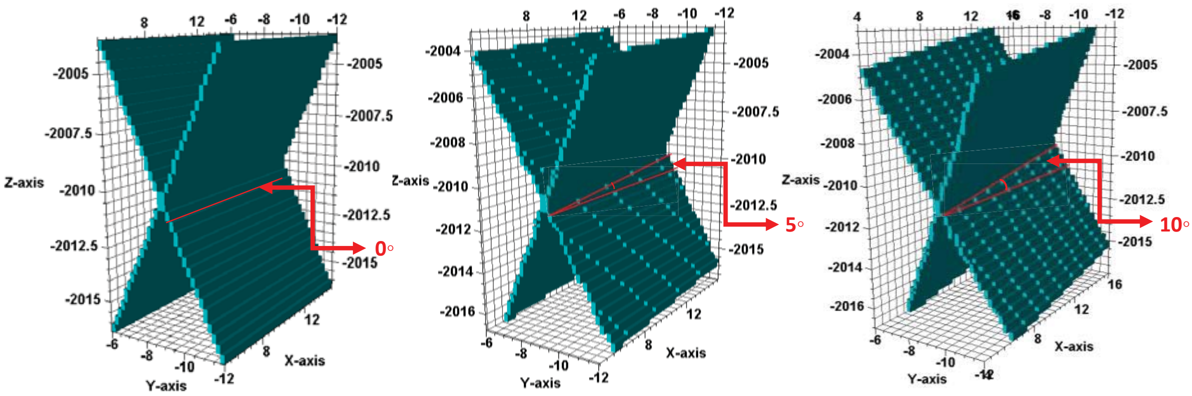

a) CASE A b) CASE B c) CASE C

Figure 7: A scenario of a single conjugate set of bands. A sandbox model with the spatial dimension of 20 m × 20 m × 20 m with a total of one million active cells (ni=100, nj=100, nk=100) was constructed. Two inclined planes (conjugate deformation bands) in opposite directions which are mutually cross-cutting were included in the model (shown in dark green). Three structures with varying hinge-line plunge were considered in the sensitivity study of Section 4.1: a) Intersection angle with the horizon is zero; b) Intersection axis is at an angle of 5^o; and c) Intersection axis is at an angle of 10^o. The angles are shown in red.

Table 1: Grid Properties and well locations in the study of one set.

Property	Value
Model dimension	20 m × 20 m × 20 m
Number of Cells	ni=100, nj=100, nk=100
Average cell size	20 cm x 20 cm x 20 cm
Injectors' location	INJ1= (i=50, j=50) INJ2= (i=51, j=50) INJ3= (i=50, j=51) INJ4= (i=51, j=51)

Given that in real-world situations deformation bands do not generally occur as isolated sets but in dense clusters, a second set of model runs (Section 5) were configured to investigate the effects of deformation band density, orientation, distribution and petrophysical properties. For this part of the study, 3D static models with a spatial dimension of 100 m × 100 m × 100 m with 125,000 active cells (ni=50, nj=50, nk=50) were generated (**Fig. 8**). To incorporate clusters of deformation bands into the models, a discrete fracture network was created using the stochastic method but guided and constrained by available outcrop data. It was assumed that the deformation bands were present throughout the permeable reservoir sandstone but did not extend into the low-porosity caprock. This step was followed by assigning the density of the deformation bands. The sensitivity study of the deformation band density is presented in Section 5.1. The shape and length of the deformation bands needed to be specified in Petrel. We assumed that the deformation bands were close to square in all the models. The orientation of the bands (dip, dip azimuth, etc...) also needed to be assigned in the modelling. Various scenarios considering different band orientations were also investigated (sensitivity analysis of section 5.3). Assigning the permeability of the bands was the last step in creating a discrete fracture network (sensitivity analysis of Section 5.2). In this sensitivity study, permeability contrasts of up to six orders of magnitude were considered. All contrasts are presented in **Table 6** and **Figure 6.** The scale-up fracture network process then converted the fracture network model into the properties that were essential for the simulator. The upscaled results were exported and used for the flow simulation in ECLIPSE 300.

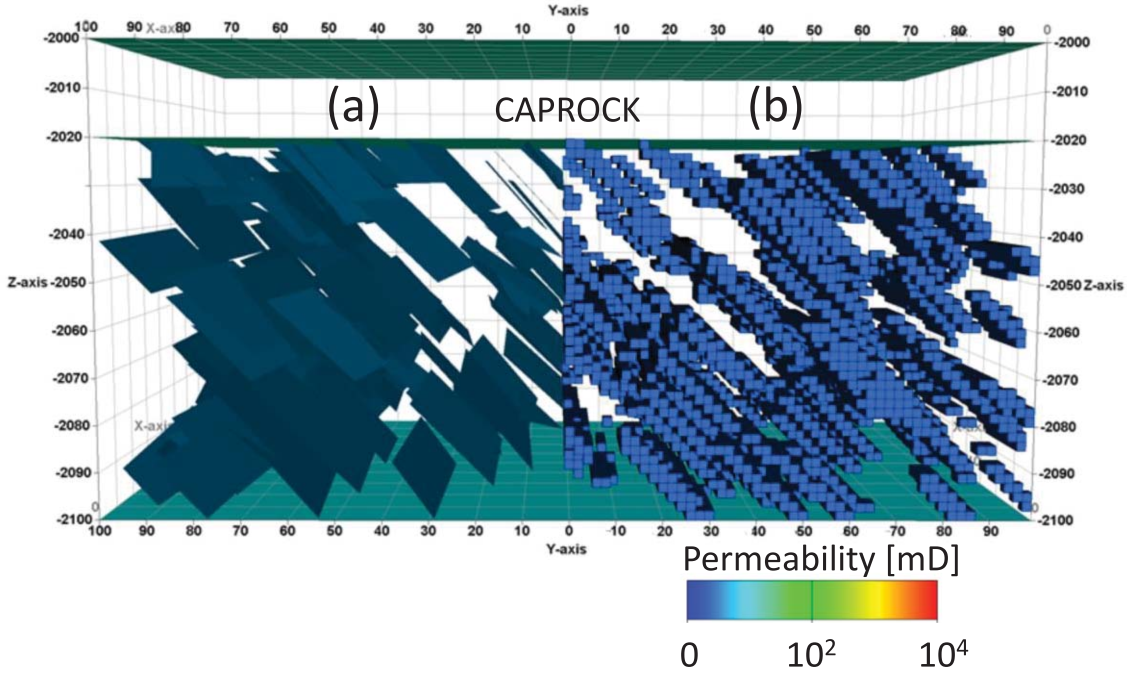

Figure 8: Models in the study of the clusters of the bands had a spatial dimension of 100 m × 100 m × 100 with 125,000 active cells (ni=50, nj=50, nk=50). Medium density parallel bands scenario is shown here. (a) Deformation bands' planes generated using fracture network model (b) Fracture network model was imported in scale up fracture network. The 3D grid form which it was generated will automatically be chosen to upscale into. As it is shown in this figure, deformation bands are dying out towards the caprock. The high permeability host rock is not shown. Low permeability bands are in dark blue. Various sensitivity scenarios including deformation band density (high, medium and low) (Section 5.1, Table 5), permeability contrasts (Section 5.2, Table 6), and orientation of the bands (parallel, random and conjugate sets) (Section 5.3) were used to study the clusters of deformation bands. These scenarios are not included in this figure.

3.1 Flow modelling

The depth of burial in much of northern England is the subject of debate (Turner et al. 1995), with the Vale of Eden supposedly being buried up to ≤ 3 km during the early Tertiary (Lewis et al. 1992). Thus, the depth of the reservoir model was set at 2000 metres with the injected CO_2 in the supercritical state. Dynamic modelling was conducted under an initial pressure of 21.4 Mpa (pressure gradient of 10.7 Mpa/Km at a salinity of 100,000 ppm) and at isothermal conditions of 65°C (using a temperature gradient of 25°C/km). It was initially assumed that the reservoir was fully saturated with brine (100% water saturation). To maintain geomechanical stability and avoid damage to the reservoir, it was assumed that the pressure remained below 75% of the lithostatic pressure gradient (22.5 Mpa/Km) at any point within the model (Noy et al. 2012). As models were constructed as "closed" aquifers, the pressure build-up constrains capacity (Mathias et al. 2011). The injectors were controlled by the surface rate with a maximum pressure limit of 34 Mpa. The same fluid properties were used for all the models. The relative permeability curves **(Fig. 9)** were taken from Onoja and Shariatipour (2018), while no hysteresis in relative permeability was considered in this study. The dynamic modelling details are summarised in **Table 2.**

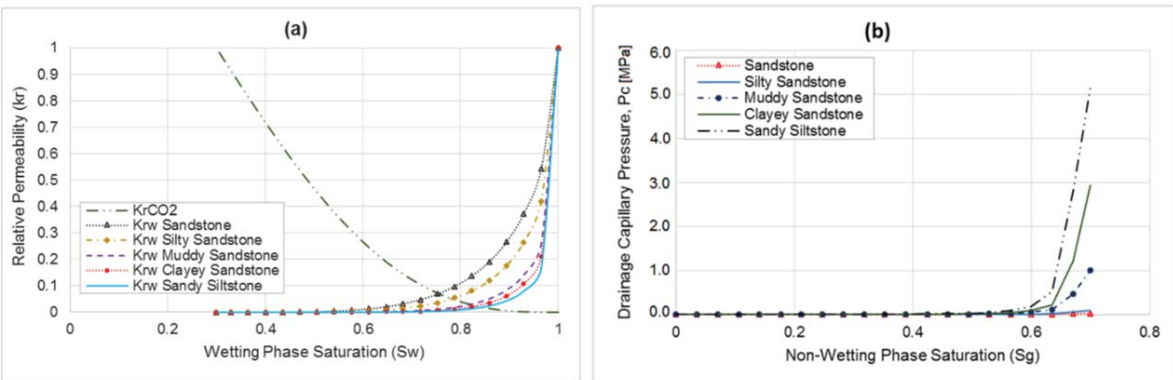

Figure 9: (a) Drainage relative permeability curve and (b) Drainage capillary pressure curve (Onoja and Shariatipour 2018).

Table 2: Parameters used for flow simulation.

Parameter	Value
Temperature at datum [°C] (Thermal gradient 25°C/km)	65
Pressure at datum [Mpa] (pressure gradient of 10.7 Mpa/Km)	20.4
Salinity (Nacl) [ppm]	100,000
Irreducible brine saturation (S_{wir})	0.3
Maximum brine saturation	1.0
End-point relative permeability to brine	1.0
End-point relative permeability to CO_2	1.0

4 Sensitivity design for one conjugate set

This part of the work examined how changing two parameters of a conjugate set might impact CO_2 distribution, namely changing the plunge angle of the hinge line between two inclined deformation bands that mutually cross-cut each other and the permeability contrast between the deformation bands and the host rock.

Four vertical CO_2 injection wells were added for the sake of symmetrical CO_2 migration and completed at layers 65 to 70 (**Table 1**). CO_2 was injected over 10 days, followed by a one year post-injection period used to study the CO_2 plume migration.

4.1 Sensitivity to variation in the hinge-line plunge

Deformation bands within the aeolian Penrith Sandstone, and many other comparable high-porosity sandstones, generally occur as conjugate sets consisting of two intersecting planes of opposing dip azimuth (Fossen et al. 2017) **(Fig. 3a).** While most attention has focussed on the magnitude and tectonic significance of the dihedral angle between the two inclined planes (Fossen et al. 2017), it is likely that the plunge angle of the hinge line between two inclined planes could also vary with respect to the horizon, either because of syntectonic processes or caused by the subsequent tilting of the entire geological formation. In most geological outcrops, this parameter is extremely difficult to measure directly but might impact storage potential by allowing CO_2 to spill from the closure formed beneath the intersecting planes. Three scenarios were investigated to test the impact of varying hinge-line plunge on flow (**Table 3**): the hinge line was horizontal (CASE A); the hinge line dips at an angle of 5° (CASE B); and the hinge line dips at an angle of 10° (CASE C), shown in **Figure 7.** For comparative purposes, one model was also run in which the geology was entirely homogeneous and contained no deformation bands (CASE D).

The dimensions of the planes representing the deformation bands were set at 10 m in a horizontal direction, 12.5 m in a vertical direction and had a thickness of 20 cm. As acknowledged in other studies (e.g., Fowles and Burley 1994), true dimensions are generally difficult to determine with any accuracy from most two-dimensional outcrops and are probably highly variable depending on the often high connectivity of individual deformation bands. These nominal dimensions, however, seemed reasonable based on the outcrop evidence and the published data (Fossen et al. 2007). A typical arrangement of deformation bands is in conjugate sets with a dihedral angle of around 45 degrees. Therefore, the acute angle of intersection between two deformation bands was set at 45° (observed at the outcrop), which also represents a typical mid-range value for conjugate sets of compactional deformation bands in an extensional basin settings (Fossen et al. 2017). For all the model runs, the permeability of the deformation bands and the host rock was set at 0.22 mD and 646 mD, respectively **(Table 3).** The domain had a pore volume of 2.288×10^3 m^3. The conjugate set provided an enclosed pore volume of 50 m^3 and was assumed to act as a local structural trap.

Table 3: Sensitivity case studies designed to test variation in the hinge-line plunge.

	Intersection angle	Deformation band		Host rock	
		Porosity [%]	Permeability [mD]	Porosity [%]	Permeability [mD]
CASE A	0^{o}	7.23	0.22	28.6	646
CSAE B	5^{o}	7.23	0.22	28.6	646
CASE C	10^{o}	7.23	0.22	28.6	646
CASE D				28.6	646

4.2 Sensitivity to the permeability contrast

To test the impact of varying the permeability contrast between the conjugate set and the host rock in the context of CO_2 storage, models were run that varied the permeability of both. Case A in the previous section, in which the axis of intersection between the two inclined deformation bands that mutually cross-cut each other was horizontal, was used to conduct this sensitivity study. Four cases were thus created: A-1, A-2, A-3, and A-4. The porosity and permeability values for both the conjugate set and the host sandstone in each scenario are summarised in **Table 4.**

Table 4: Sensitivity case studies designed to test permeability contrast.

	Deformation band		Host rock	
	Porosity [%]	Permeability [mD]	Porosity [%]	Permeability [mD]
CASE A-1	7.23	0.22	28.6	646
CSAE A-2	9.82	0.91	29.9	770
CASE A-3	5.86	0.24	18.6	41
CASE A-4	7.74	0.85	18.7	29

5 **Sensitivity design for clusters of deformation bands**

In most geological settings, deformation bands do not occur as single isolated features, but as dense clusters (**e.g., Fig. 4**). In extensional tectonic settings, dense clusters of deformation bands may occur in a linear zone that extends from the tips of laterally propagating normal faults (Fossen et al. 2007). The deformation bands are a precursor to the development of a through-going slip surface on a normal fault. As this develops, the deformation bands will ultimately form a damage zone on either side of the main fault plane. **Fig. 4** provides an illustration of this scenario from the Penrith Sandstone with a high density of deformation bands located on either side of a slip surface that has developed on the outer face of a thick zone of granulation seams **(**see **Fig. 3c)**. Similarly, measurements of deformation bands in the Wingate Sandstone, Colorado National Monument (Jamison and Stearns 1982) and Moab Member, Entrada Sandstone (Antonellini and Aydin 1994) show a clear correlation between the high density of the deformation bands and their proximity to the fault. Schueller et al. (2013) identified a logarithmic decrease in the number of deformation bands away from the fault core.

The simulation studies in this section examine the influence of clusters of deformation bands on CO_2 storage capacity and security. In particular, we wanted to examine:

1. The effects of varying the number of deformation bands;
2. The effects of varying the permeability contrast between the host rock and dense clusters of deformation bands;
3. The impact of introducing a high transmissibility fault into dense clusters of deformation bands, simulating the common scenario found in extensional basin settings where the deformation bands occur in a damage zone around a fault.

One injector well was placed in the centre of the model. The location of the injector was chosen to maximise the volumetric sweep efficiency and was placed away from the boundaries. CO_2 was injected for eight years, followed by a two year post-injection period to study the CO_2 plume migration. The same dynamic properties as outlined in **Table 2** were applied.

5.1 Deformation band density

Deformation bands have to be abundant in order to have any significant influence on fluid flow (Fossen and Bale 2007; Rotevatn et al. 2009). Three models with different number of deformation bands were considered using frac count/volume in Petrel. The three cases are identified by the label “H” (high deformation band density, six per metre), “M” (medium deformation band density, three per metre), and “L” (low deformation band density, one per metre). This range was also proposed by Aydin (1978) for deformation bands in aeolian sandstone. Deformation bands in cases of “H” might be considered representative of a geological scenario proximal to a normal fault, while those labelled “L” might be more distal to a fault.

For each case, deformation bands with different distribution pattern were modelled using parallel, random and conjugate sets. An un-deformed control case was labelled “U”; hence, 13 cases were investigated. The permeabilities of the deformation bands and the host rock were set at 0.91 mD and 770 mD, respectively **(Table 5).** The objective of this section is to investigate how density of deformation bands influences the CO_2 storage security and capacity. H-CON0 broadly replicates the type of geological scenario observed in the Penrith Sandstone (see **Fig. 4**).

Table 5: Models built to study the effects of density of deformation bands on CO_2 distribution. L refers to low density, M to medium density and H to high density of deformation bands. PARA refers to the parallel distribution of deformation bands and RAND refers to the random distribution of deformation bands. In CON0 the conjugate sets had a horizontal intersection axis. In CON10 this angle was 10. U refers to the un-deformed model.

Number of deformation band patches in each case	**Features distribution**	**Permeability [mD]**		**Cases name**
		Deformation band	Host rock	
Low	Parallel	0.91	770	L-PARA
	Random	0.91	770	L-RAND
	Conjugate 0	0.91	770	L-CON0
	Conjugate 10	0.91	770	L-CON10
Medium	Parallel	0.91	770	M-PARA
	Random	0.91	770	M-RAND
	Conjugate 0	0.91	770	M-CON0
	Conjugate 10	0.91	770	M-CON10
High	Parallel	0.91	770	H-PARA
	Random	0.91	770	H-RAND
	Conjugate 0	0.91	770	H-CON0
	Conjugate 10	0.91	770	H-CON10
None			770	U

5.2 Host rock and deformation band permeability contrast

Eight different scenarios were considered in this section, in order to investigate the effects of permeability contrast on CO_2 storage capacity and security. The permeability of the host rock was increased from 10 mD in PC1 to 10,000 mD in PC4, while the permeability of the deformation bands remained constant (at 0.01 mD). In addition, four other models with permeability contrasts of one to three orders of magnitude were considered. The values from

Penrith Sandstone (**Fig. 6 Table 6**) and the literature (e.g., Torabi et al. 2008) were covered. Medium density deformation bands were used for all flow modelling, consequently, all cases were assigned with the label M. Also, eight undeformed cases were used for comparative purposes (UNDEFORMED-1 to UNDEFORMED-8). The permeability of the deformation bands and host rock are presented in **Table 6**. One dipping high transmissibility fault, with an assumed permeability of 2000 mD and transmissibility of 34.108 cP.rm^3/day/bars, was placed in all cases.

5.3 Deformation band geometry and location against high transmissibility fault

In extensional settings, deformation bands generally occur in association with normal faults. It is important to investigate if their arrangements and distributions can affect fluid flow (Fossen and Bale 2007). To cover a range of structural possibilities, five models were considered which varied the orientation of the deformation bands relative to the transmissive fault plane **(Fig. 10)**. This section describes how this geological scenario might influence storage security. Medium density of deformation bands (three per metre) was used in all cases. The permeabilities of the deformation bands and the host rock were set at 0.91 mD and 770 mD, respectively.

Table 6: Permeability values used for the permeability contrast sensitivity study. M refers to medium density of deformation bands and PC refers to permeability contrast.

Features shape	Permeability [mD]		Cases name
	Host Rock	Deformation band	
Conjugate (angle of 0^{o})	10	0.01	M-CON0-PC1
	100	0.01	M-CON0-PC2
	1000	0.01	M-CON0-PC3
	10000	0.01	M-CON0-PC4
	646	0.22	M-CON0-PC5
	770	0.91	M-CON0-PC6
	41	0.24	M-CON0-PC7
	29	0.85	M-CON0-PC8
Conjugate (angle of 10^{o})	10	0.01	M-CON10-PC1
	100	0.01	M-CON10-PC2
	1000	0.01	M-CON10-PC3
	10000	0.01	M-CON10-PC4
	646	0.22	M-CON10-PC5
	770	0.91	M-CON10-PC6
	41	0.24	M-CON10-PC7
	29	0.85	M-CON10-PC8
Parallel	10	0.01	M-PARA-PC1
	100	0.01	M-PARA-PC2
	1000	0.01	M-PARA-PC3
	10000	0.01	M-PARA-PC4
	646	0.22	M-PARA-PC5
	770	0.91	M-PARA-PC6
	41	0.24	M-PARA-PC7
	29	0.85	M-PARA-PC8
Perpendicular	10	0.01	M-PERP-PC1
	100	0.01	M-PERP-PC2
	1000	0.01	M-PERP-PC3
	10000	0.01	M-PERP-PC4
	646	0.22	M-PERP-PC5
	770	0.91	M-PERP-PC6
	41	0.24	M-PERP-PC7
	29	0.85	M-PERP-PC8
Random	10	0.01	M-RAND-PC1
	100	0.01	M-RAND-PC2
	1000	0.01	M-RAND-PC3
	10000	0.01	M-RAND- PC4
	646	0.22	M-RAND-PC5
	770	0.91	M-RAND-PC6
	41	0.24	M-RAND-PC7
	29	0.85	M-RAND-PC8

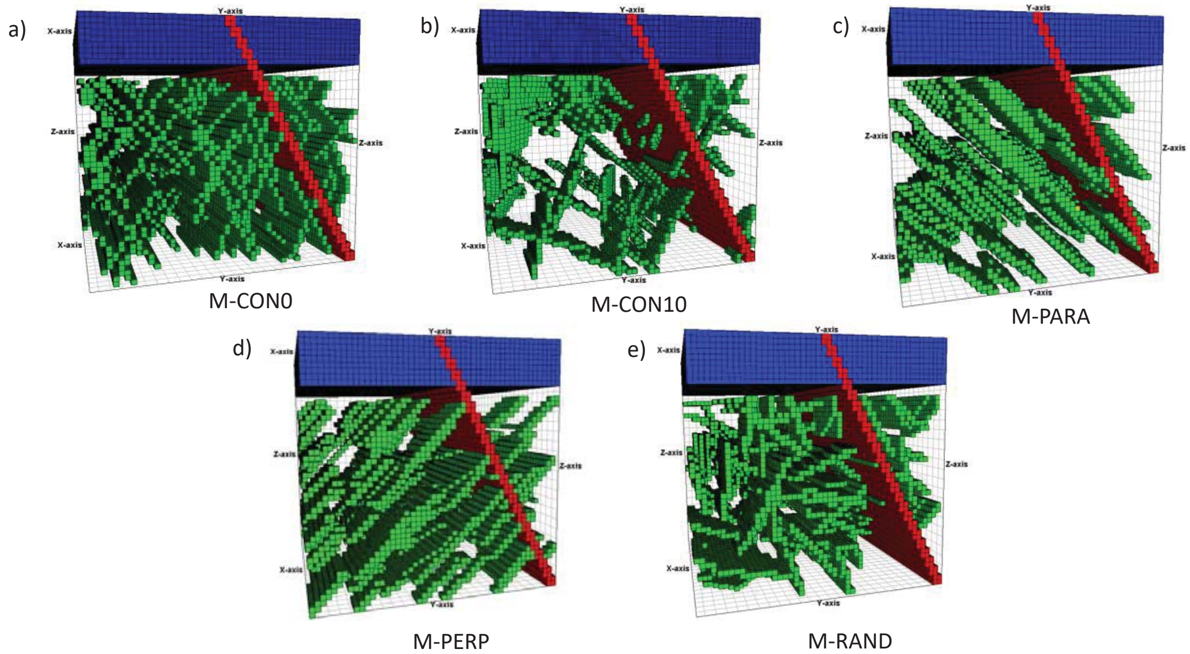

Figure 10: Five cases were studied here: a) Conjugate sets of deformation bands with 0 degrees intersection angle, b) Conjugate sets of deformation bands with 10 degrees intersection angle, c) Parallel set of deformation bands which are parallel to the fault, d) Parallel set of deformation bands which are perpendicular to the fault and e) Randomly distributed deformation bands (Blue: caprock, Red: fault, Green: deformation bands).

5.4 Injection rate and well location

The cases introduced in Section 5.3 were used and three injection rates were applied for each case. An injector was placed in the centre of the models. The cases with “LR” had a low injection rate (100 sm^3/day), “MR” had a medium injection rate (250 sm^3/day) and “HR” had a high injection rate (525 sm^3/day). The highest injection rate was the maximum rate that could be used before the system reached the pressure constraint of 34 Mpa and caused damage to the reservoir. These injection rates were modelled to identify trends in mobile gas accumulation both in the fault rock and beneath the caprock.

Cases in Section 5.3 were also used to study the placement of the injector well and its effect on CO_2 storage security. Two well locations were considered. In cases with "C", the injector was centred in the model (well location: x=50 and y=50), and in cases with "F", the well was placed far from the fault (well location: x=25 and y=40). The injection rate was 250 sm^3/day.

6 **Results**

The results are presented in two subsections, namely, one conjugate set of deformation bands (6.1) and clusters of deformation bands (6.2).

6.1 One conjugate set of deformation bands

6.1.1 The effects of intersection angle on CO_2 distribution

The storage capacity of each set is a function of host rock porosity and the conjugate set closure size. The upward movement of CO_2 is driven by the buoyancy contrast between the lighter CO_2 and the denser formation brine. When a conjugate set was introduced into the model it filled with CO_2 up to its spill point, then gas escaped in the X direction **(Fig. 11a, b** and **c)** and ascended towards the upper layers. In CASE A **(Fig. 11a),** the CO_2 plume showed a symmetrical distribution along the intersection axis. In the models where the conjugate set had a tilted intersection (cases B and C), the CO_2 plume tended to migrate up-dip along the intersection axis whilst under buoyancy, resulting in an asymmetrical plume along the axis **(Fig. 11b, c).** In the homogenous CASE D**,** with no deformation band, the CO_2 plume was migrated vertically and was distributed symmetrically around the injection well **(Fig. 11d).**

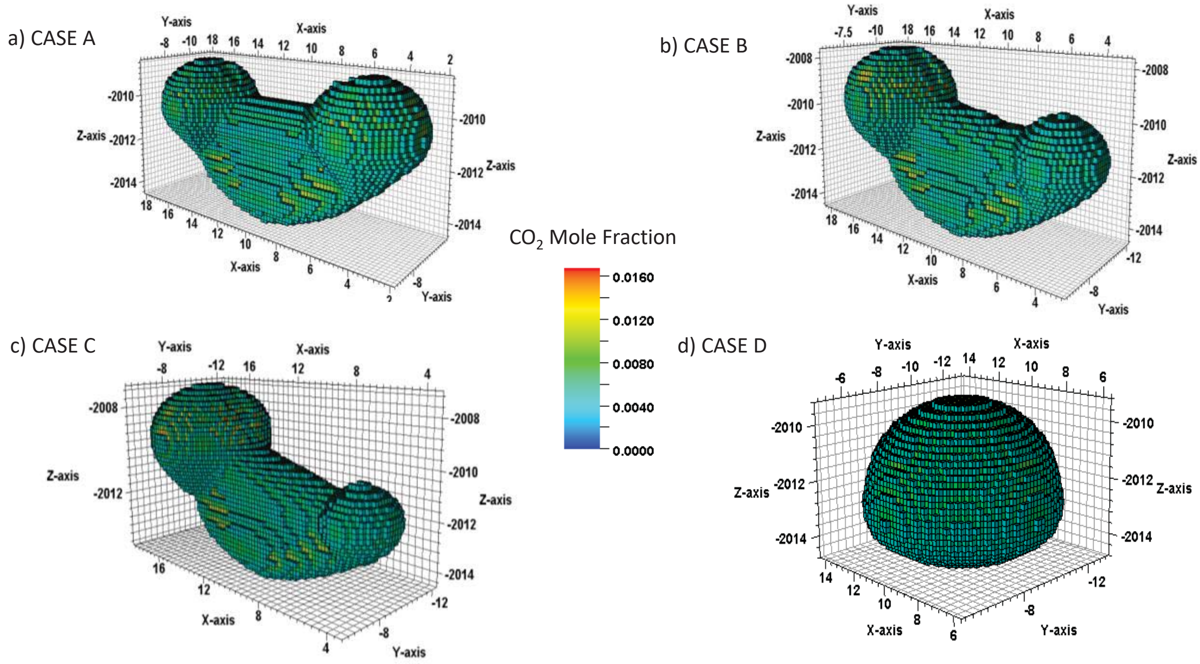

Figure 11: Effect of intersection angle on CO_2 distribution. In cases A, B and C, the conjugate set filled with CO_2 up to its spill point, then the gas escaped in the X direction and ascended towards the upper layers. The homogenous model (CASE D) shows a symmetrical CO_2 plume around the injection well. See **Table 3** for the input data.

6.1.2 The effects of host rock-deformation band permeability contrast on CO_2 distribution

Modelling results based on the typical permeability range for the host rock and deformation bands found within the Penrith Sandstone (**Table 4**) are shown in **Fig. 12.** The deformation band-host rock permeability contrast was sufficiently high to create a reliable mini-structural trap in cases A-1 and A-2 (regardless of the closure size) (**Fig. 12A**). However, deformation bands with a smaller permeability contrast can still affect flow, although they are unable to block it completely (cases A-3 and A-4) (compare with CASE D in **Fig. 11**). The CO_2 distribution across the deformation bands in these four cases is displayed in **Fig. 12B**. The amount of dissolved CO_2 in the brine was seen to be greater where the deformation bands had higher permeability and porosity. Furthermore, a high host rock permeability contributes to CO_2

trapping as dissolved CO_2 **(Fig. 13).** Aside from the CO_2 that became structurally trapped in the host rock in the closure beneath the intersecting plane, the properties of the host rock influenced the CO_2 storage capacity and security by changing the amount of the CO_2 that could be dissolved in the water phase.

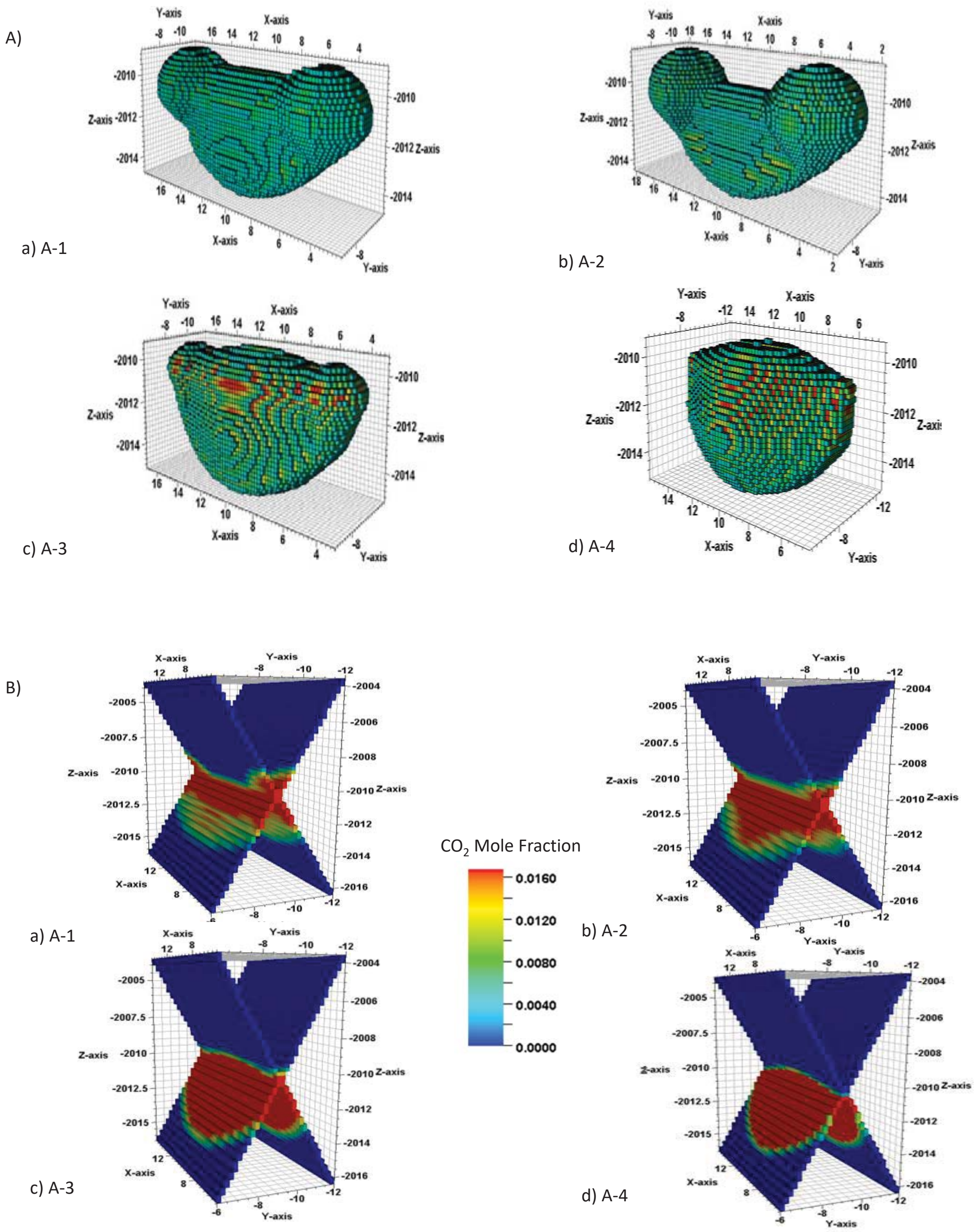

Figure 12: A) Effect of deformation band-host rock permeability contrast on CO_2 distribution. B) CO_2 distribution across the deformation bands (see **Table 4** for the permeability values).

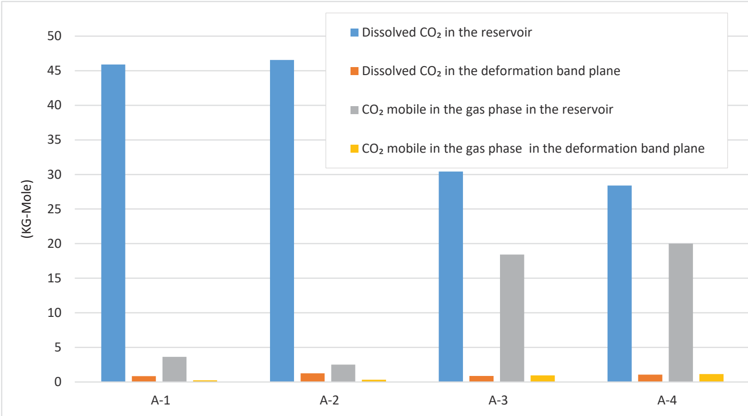

Figure 13: Dissolved and mobile CO_2 in the reservoir and along the bands at the end of the simulation period. See Figure 12 for associated models and Table 4 for the porosity and permeability values.

6.2 Clusters of deformation bands

6.2.1 The effects of deformation band density on CO_2 storage

In the un-deformed case (U) the resultant plume was uniform and symmetrical. **Figure 14A** and **B** illustrate the density of deformation bands and CO_2 distribution in the case of low density (L-CON10), medium density (M-CON10) and high density (H-CON10) of conjugate sets of deformation bands. The impact of deformation band density on plume geometry was apparent. As the number of deformation bands increased in the model, the vertical and lateral movements became restricted and the plume became progressively distorted. Less CO_2 reached the caprock where there was a higher number of deformation bands. More mobile gas was observed beneath the caprock in the homogeneous model and the runs with a low to medium number of deformation bands **(Fig. 14** and **Fig. 15).**

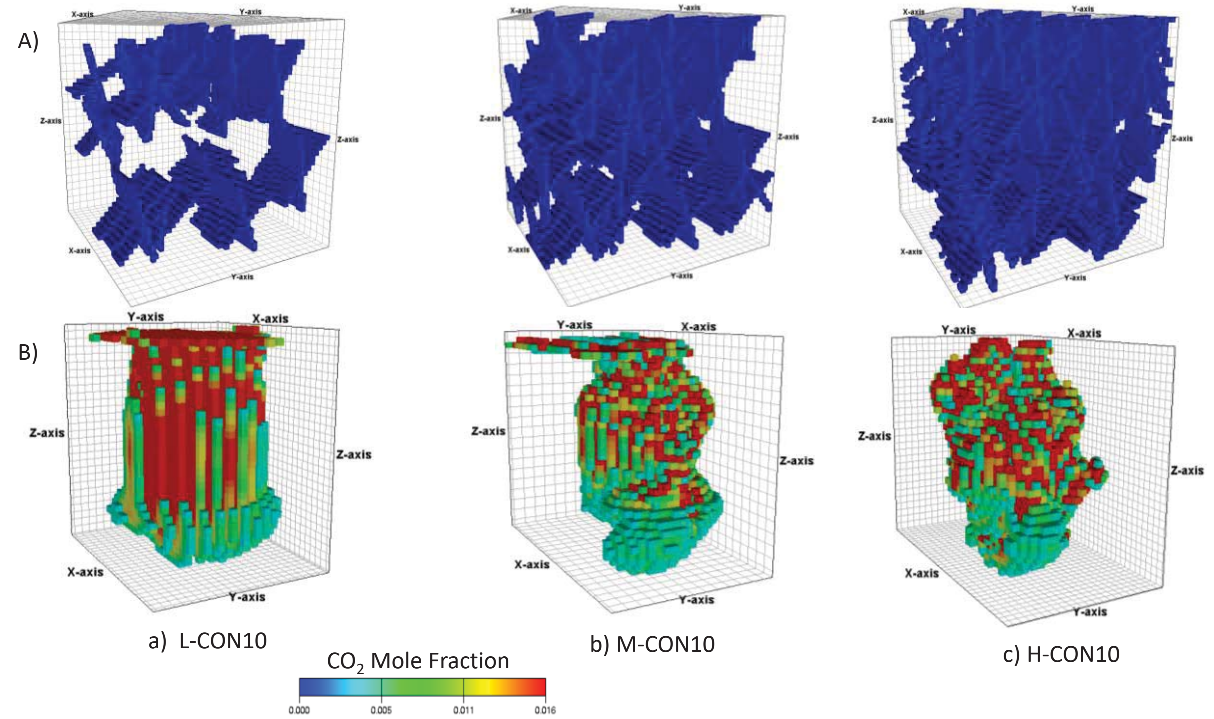

Figure 14: A) Low, medium and high density of deformation bands. The fault is not shown here. B) Effect of density of deformation bands on flow distribution.

The volumes of dissolved CO_2 in brine, and the mobile CO_2 in both the reservoir and beneath the caprock are shown in **Figure 15**. Although insignificant, the greatest amount of CO_2 dissolved in the water phase and the lowest degree of mobile CO_2 were observed in the homogeneous model (U), and in models with low deformation band density. The amount of free gas beneath the caprock was lower in the models with a higher number of deformation bands.

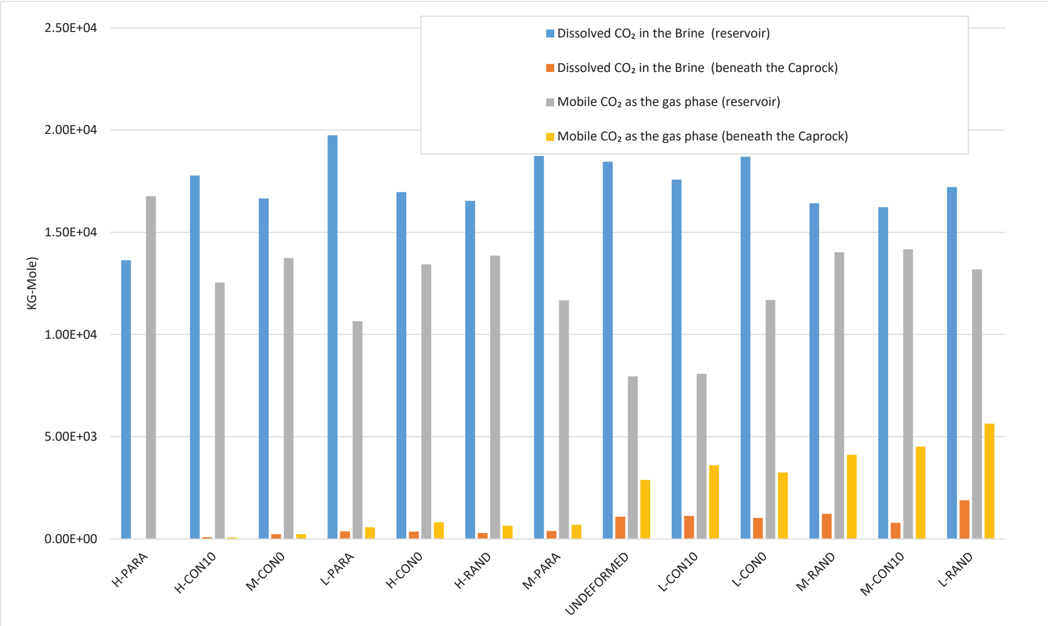

Figure 15: The amount of dissolved and mobile CO_2 in both the reservoir and beneath the caprock. More mobile gas occurred beneath the caprock in models with a low to medium number of deformation bands.

Reservoir pressure is shown in **Figure 16**. None of the runs in this section reached the failure limit of the 34 Mpa (Section 3.1), even in the scenarios with the highest number of low permeability deformation bands.

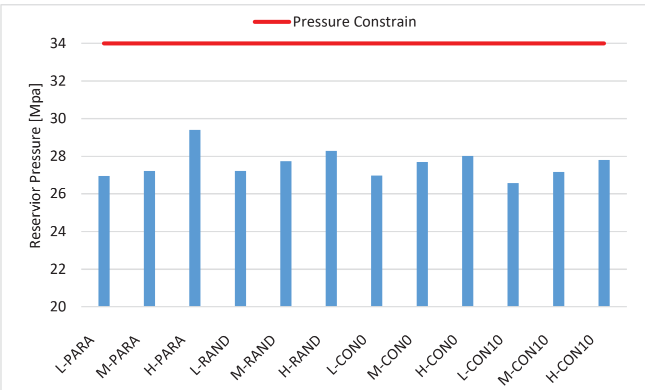

Figure 16: None of the models in the study of deformation band density reached the pressure limit of 34 Mpa. Note that the permeability contrast of three orders of magnitude were considered here.

6.2.2 The effects of host rock-deformation band permeability contrast on CO_2 storage

The dissolved and mobile gas in the storage formation, the fault rock and the layer below the caprock in models, where a permeability contrast variation between the host rock and the clusters of deformation bands exist, are illustrated in **Figure 17.** The high permeability of the host rock resulted in a higher dissolved CO_2 content as a result of increased brine and CO_2 interaction (e.g., M-PERP-PC4). Consequently, the highest mobile CO_2 in the models was observed in the reservoirs with a low permeability host rock (e.g., M-CON0-PC1). The shape of the modelled deformation bands had no significant effect on the amount of dissolved CO_2 in either the brine or the mobile gas in the storage formation.

During the injection and post-injection periods the highest free gas beneath the caprock was observed where the host rock exhibited a high permeability, with either a random distribution of deformation bands or conjugate sets of deformation bands (e.g., M-RAND-PC3 and M-CON10-PC5). No free phase CO_2 reached the caprock where the host rock had a low permeability (e.g., M-PARA-PC1).

An insignificant amount or no free gas was detected in the fault rock where deformation bands were parallel to the transmissible fault (e.g., M-PARA-PC4). Cases with a perpendicular distribution of deformation bands against the fault were among those with the highest amount of free gas in the fault rock (along with CON10). Even in M-PEPR-PC1, PC2 and PC7 (low permeability host rock), free CO_2 reached the fault plane. The earliest breakthrough of CO_2 to the caprock and the leaky fault occurred in PERP cases where the host rock had a high permeability. This is because the CO_2 plume was directed towards the caprock and fault by i) buoyancy forces; ii) the presence of a perpendicular set of deformation bands; while iii) the high permeability of the host rock increased CO_2 flow velocity.

The CO_2 distribution in cases with conjugate and paralleled deformation bands are illustrated in **Figure 18**. One large, sub-symmetrical plume formed around the injector and migrated upwards due to buoyancy forces (in all PC1 and PC8 cases). The plume shapes lacked radial symmetry and were irregular in cases with a higher permeability contrast (in all PC3, PC4, PC5 and PC6 cases). The impact of the deformation bands on the flow was significant in these cases. The overall shape of the plume changed as deformation bands varied, regardless of density and permeability contrast (compare **Figs. 18A** and **18B**).

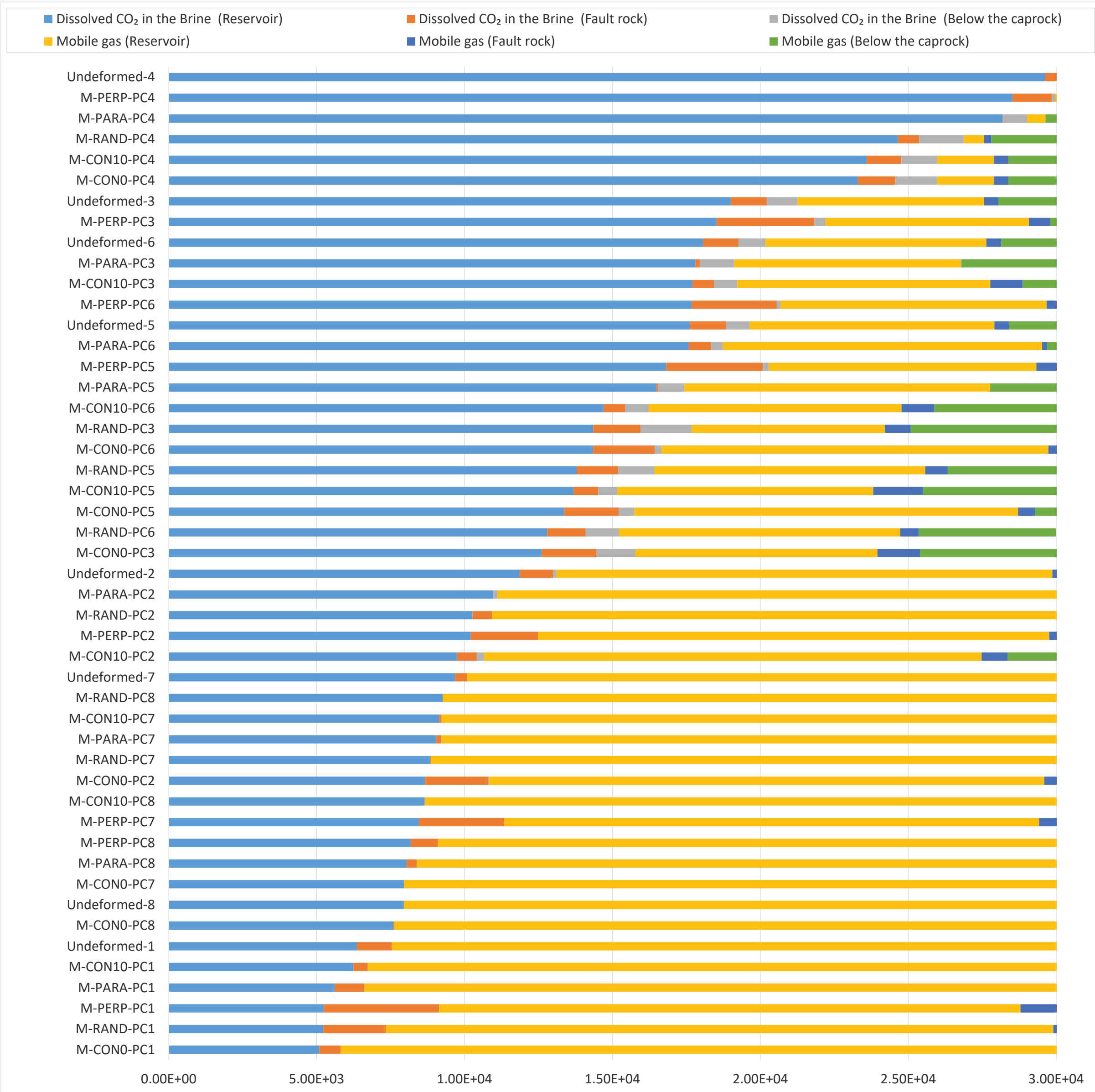

Figure 17: Dissolved CO_2 and mobile gas in the reservoir, in the fault rock and in the layer below the caprock. M refers to a medium number of deformation bands. PERP refers to a parallel set of deformation bands that are perpendicular to the fault. PARA refers to a parallel set of deformation bands that are parallel to the fault. RAND refers to a random distribution of deformation bands. CON0 refers to conjugate sets of deformation bands with a horizontal intersection axis, and the intersection axis in CON10 is at an angle of 10°. PC denotes permeability contrast. For the permeability values see **Table 6**.

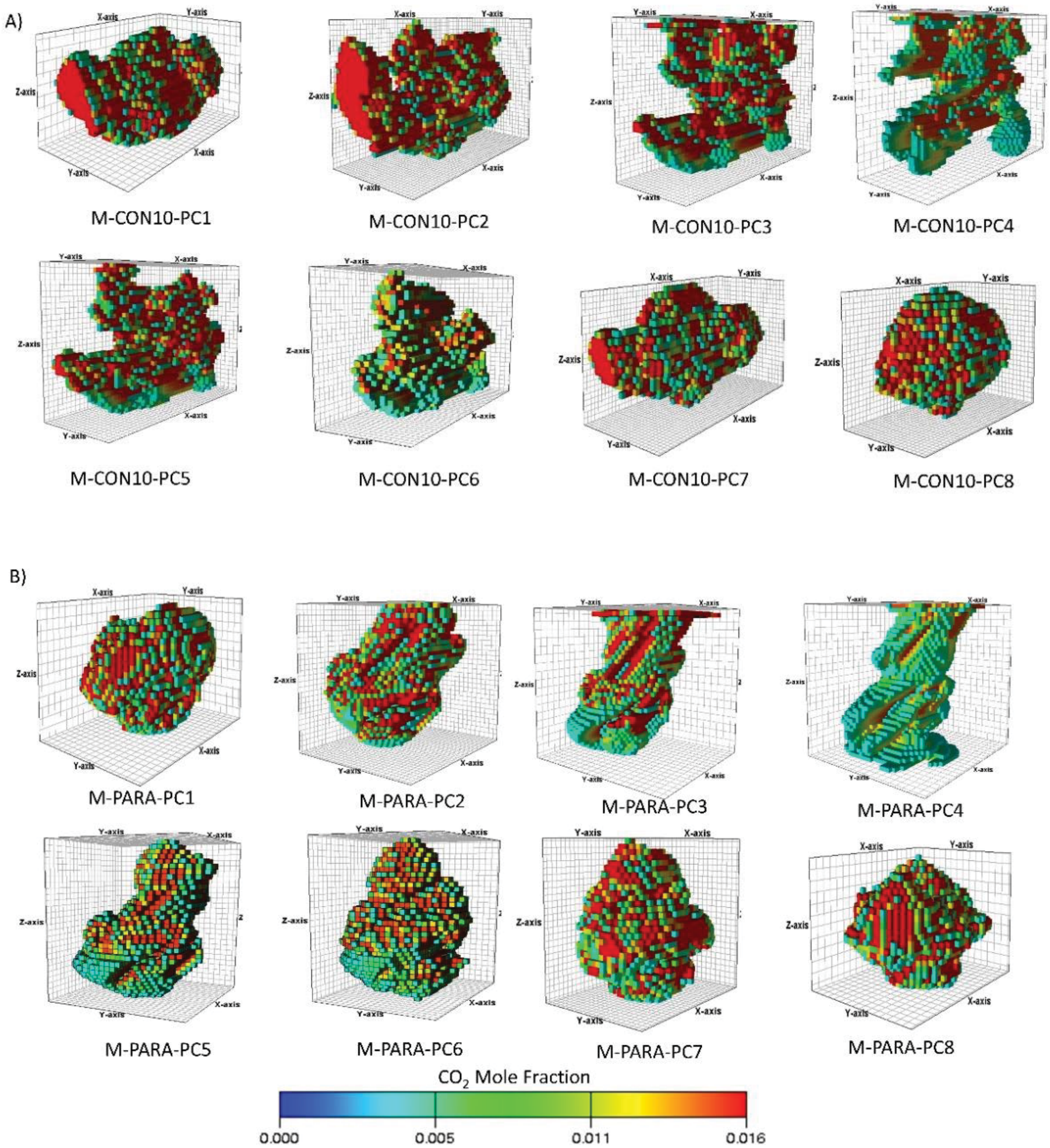

Figure 18: CO_2 distribution in cases with differing permeability contrast. A) CO_2 distribution in models with conjugate sets of deformation bands with an intersection angle of 10°; and B) CO_2 distribution in cases with a parallel distribution of deformation bands.

6.2.3 The effects of deformation band geometry and their location against a high transmissibility fault

The results for the amount of free gas beneath the caprock and in the fault, for the five cases investigating the geometry and distribution of the bands, are shown in **Figure 19**. The highest amount of mobile gas both in the fault zone and beneath the caprock was observed in M-CON10 and M-RAND. M-CON0 was the most secure model as both the free CO_2 beneath the caprock and the fault rock were relatively low. None of the model runs showed complete obstruction of CO_2 movement towards the leaky fault and the caprock. Even in the M-PARA model, when most of CO_2 redirected away from the fault, CO_2, as free gas, was still detected in the fault plane. This is because a medium density of deformation bands was used in the modelling study in this section.

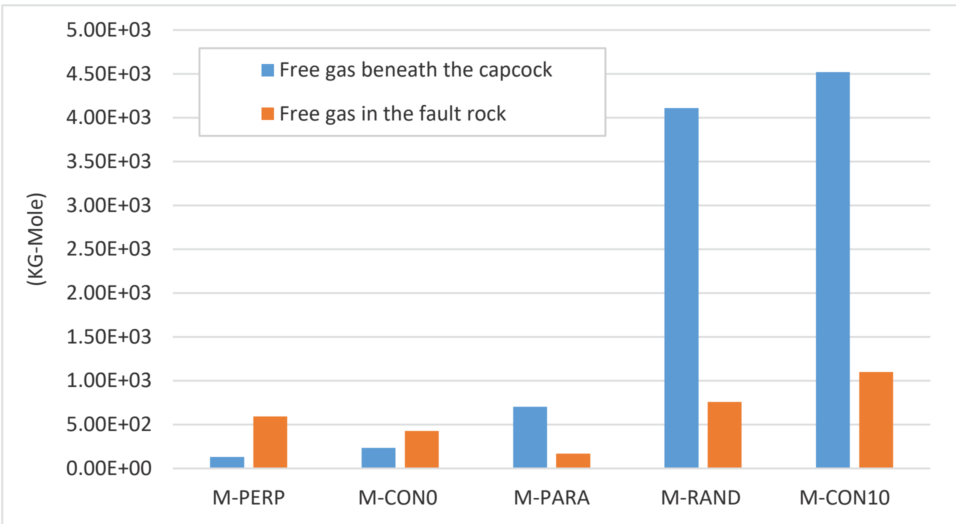

Figure 19: The amount of free gas beneath the caprock and in the fault rock, in cases with different deformation band geometry.

6.2.4 The effects of injection rate and well location on CO_2 storage security

As observed in the previous study, M-RAND and M-CON10 appeared to be the least secure in regard to CO_2 retention. Outcomes were repeated at high, medium and low injection rates. These two cases, again, had the highest free gas accumulation at the top of the reservoir across all three injection rate scenarios and are the least secure configurations for CO_2 storage (**Fig. 20**). The most secure cases were models with sets of conjugate deformation bands with a horizontal intersection angle. Models with perpendicular distribution against the fault did not follow the trends discussed above. While low and medium injection rates were amongst the most secure cases, a high injection rate indicated a high volume of free gas beneath the caprock, as more CO_2 was directed towards the fault. CO_2 had moved upwards via the fault and ultimately accumulated with the CO_2 that had already reached the caprock.

The optimum injection rate is of key importance for the types of reservoirs studied herein. With high injection rates the CO_2 may leak through proximal high transmissibility faults, thus limiting the storage effectiveness and diminishing injection security. In addition, deformation band density and permeability contrast also need to be taken into consideration, as cases with a high number of deformation bands, in low permeability host rock, can lead to injectivity issues and potential project failure.

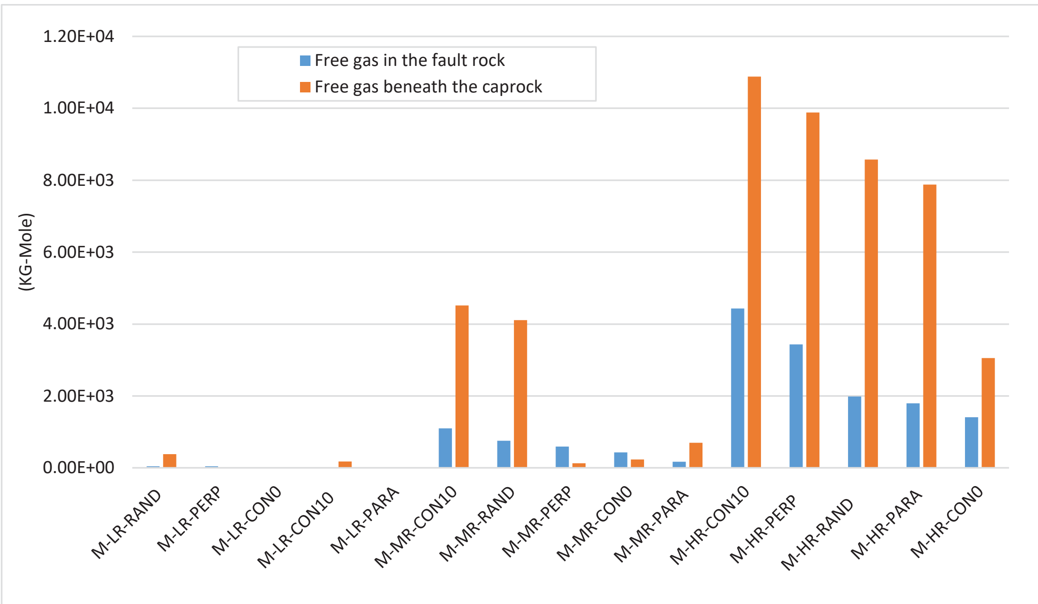

Figure 20: The amount of free gas beneath the caprock and in the fault rock in different injection scenarios display similar trends. M refers to a medium density of deformation bands,

LR refers to a low injection rate, MR to a medium injection rate and HR to a high injection rate.

The amount of mobile gas in the caprock, in cases where the well was far from the fault was less than when the well was placed in the centre of the model, as free phase CO_2 was unable to reach the fault. Clearly, well placement has a considerable effect on CO_2 storage security and can help guarantee safer storage by avoiding any faults in the vicinity of the injection wells **(Fig. 21).**

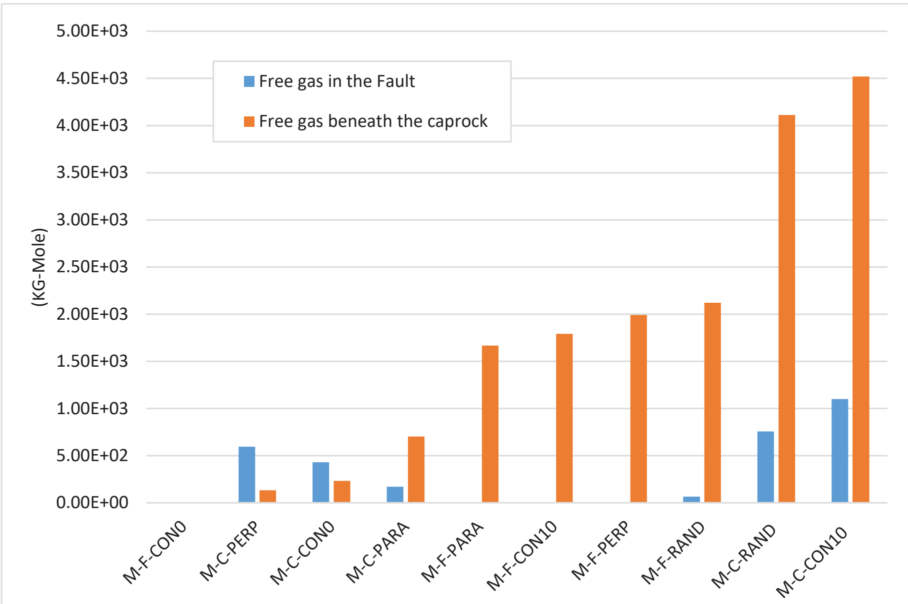

Figure 21: Amount of free gas beneath the caprock and in the fault rock in different well placements. M refers to models with a medium density of deformation bands, F refers to the models with a well placement in x=25 and y=40 and C refers to the models with a well placement in x=50 and y=50.

7 **Discussion**

The discussion demonstrates this study's similarities to the conclusions of other researchers in the field (Fossen and Bale 2007; Rotevatn et al. 2009; Fachri et al. 2013; Zuluaga et al. 2016; Rotevatn et al. 2017). Nevertheless, some results contrast with these pre-eminent authors, as we considered a different fluid type (injecting supercritical CO_2 into saline aquifers) and a wider range of host rock permeabilities.

7.1 Deformation band density

Fachri et al. (2013), Rotevatn et al. (2009) and Fossen and Bale (2007) have previously indicated that a significant concentration of low permeability bands is needed for deformation bands to have considerable negative effects on productivity. This is because the abundance of these structural heterogeneities, which can extend to tens or hundreds of metres (Aydin 1978) with various orientations (Rotevatn et al. 2009), may cause extensive compartmentalisation and represents a major barrier to fluid flow. In the CO_2 storage context, for deformation bands to contribute to secure storage, a number of deformation bands that do not overly damage reservoir communication nor reduce bulk porosity, that improves the sweep efficiency, block the upward movement of CO_2, and do not cause injectivity issue is necessary. As pressure buildup is sensitive to reservoir permeability, an exceptionally high number of low permeability bands will cause injectivity issues. In this study, the number of deformation bands observed at the Penrith Sandstone outcrop (reported also by Aydin (1978) for deformation bands in aeolian sandstone), and modelled with three orders of magnitude permeability contrast, did not cause injectivity issues but can contribute to the secure storage of CO_2. In the case of extensional settings these structures can improve security, as high density deformation bands occur in the proximity of the fault. In this study, a higher density of deformation bands decreased the amounts of free gas beneath the caprock and in the fault plane and delayed the CO_2 arrival time to the top of the reservoir. However, reservoir communication was slightly impaired, resulting in an insignificantly lower volume of CO_2 being dissolved in the water phase. As CO_2 could not reach all parts of the reservoir there was less CO_2 and brine interaction. This produced results in contrast to the study of Zuluaga et al. (2016), as they had previously shown that the ability of fluids to saturate the reservoir, namely sweep efficiency, is improved by deformation band occurrence. This outcome is based on the fact that these low permeability features may redirect fluids to parts of the reservoir that would otherwise be bypassed. How the reservoir is compartmentalised by these structural features, and the difference in spatial distribution, may have had an effect on the overall sweep in this study, which can cause decreased dissolution of CO_2 in the water phase. One unexpected result was that the main portion of injected CO_2 was blocked from the caprock, not because of the conjugate shape of the deformation bands, but their density **(Fig. 15).** Consequently, when considering the role of such structural heterogeneities in reservoirs, it is important to evaluate each reservoir separately in terms of the number of the bands, their location against larger structures, their geometry, properties and continuity.

7.2 Host rock-deformation band permeability contrast

Deformation bands can substantially modify fluid flow (Antonellini and Aydin 1994). However, the extent to which these structures influence CO_2 distribution will depend on the permeability contrast between the host rock and the deformation bands (Fossen and Bale 2007; Rotevatn et al. 2009; Zuluaga et al. 2016; Rotevatn et al. 2017).

The study of one set has shown a limited but noticeable effect of deformation bands with a permeability contrast below two orders of magnitude, and the significant effect of deformation bands with a permeability contrast above three orders of magnitude. The results of the flow simulations using one set, as presented herein, have shown that a complete blockage of flow occurs, although this depends on the closure size and the permeability contrast. Our results disagreed with the study by Rotevatn et al. (2017). They showed that deformation bands with a permeability contrast of one order of magnitude less than that of a low to moderate permeability host rock had a pronounced impediment effect. Our study has shown that while one-two orders of magnitude permeability contrast affect flow, three orders of permeability contrast are needed to retard the flow effectively. This inconsistency arises from the fact that the gas reservoirs (herein, a supercritical CO_2 injection) are only sensitive to three orders of magnitude permeability differences (Ringrose and Bentley 2015; Newell et al. 2019), which differs from the fluid modelled in Rotevatn et al. (2017) (two-phase flow simulations, with water displacing oil). Consequently, the fluids under investigation are a factor that needs to be considered when studying such structural heterogeneities.

The long term CO_2 storage security of such systems depends on the amount of free gas that reaches the transmissible faults or caprock, as there is an increased risk of leakage. This is not only controlled by the permeability contrast, but also by the permeability of the host rock itself. Many researchers have not included the effect of host rock permeability in their sensitivity analyses (Rotevatn et al. 2009; Fachri et al. 2013; Zuluaga et al. 2016). The study by Rotevatn et al. (2017) on carbonate rocks considered various permeabilities for the host rock. However, as the porosity and permeability values for both the host rock and the deformation band samples were lower for the carbonate rock, their study cannot be extrapolated to a siliciclastic reservoir with very high permeabilities. In the study of clusters of deformation bands, the deformation bands permeability remained below 0.91 mD throughout, with the host rock permeability ranging from 10 to 10,000 mD (**Table 6).** The storage security was jeopardised in models where the host rock had medium to high permeability and a permeability contrast above three orders of magnitude (see models PC2-PC3-PC4-PC5, and PC6), as free gas reached the caprock and/or leaky fault. Although models with low host rock permeability have shown insignificant mobile gas beneath the caprock or the fault plane, they exhibited a higher free gas in the system. They also may cause injectivity problems in higher densities.

Fachri et al. (2013) and Rotevatn et al. (2017) argued that decreasing deformation band permeability (higher permeability contrast) results in a complex waterfront shape and slow fluid propagation. In this study, although a more tortuous flow pattern was observed in the high permeability contrast models, faster flow propagation was observed due to higher host rock permeability.

Permeability contrast is, therefore, not the only criterion that needs to be considered while injecting CO_2 into a very high permeability reservoir with deformation bands, for low-density CO_2 in such a reservoir passes such heterogeneities and can reach a caprock that may contain leakage points. In contrast to what we previously thought, conjugate sets of deformation bands did not significantly contribute to CO_2 storage security or block CO_2 in models with the high permeability host rock.

7.3 Deformation band geometry and distribution

The study of one conjugate set of deformation bands (Section 6.1) demonstrated that they can partially block the upward movement of CO_2, even where the intersection axis between the two low permeability planes is inclined. However, this depends on the injection rate, the

closure size and the permeability contrast. A higher acute intersection angle between two deformation bands would increase the pore volume available for CO_2 that could be stored as free gas and would thereby improve storage security.
Investigating the effect of deformation bands geometry (Section 6.2.3) showed that the solid geometry of deformation bands can inhibit or accentuate CO_2 migration towards the caprock or transmissible fault. This is to be expected, as the deformation bands in M-CON10 retained injected CO_2 for only a short time period. The CO_2 then migrated along the intersection angle to eventually reach the caprock or transmissible fault. In cases where the deformation bands were randomly distributed, the free movement of CO_2 occurred in some parts of the reservoir where sufficient gaps allowed for a possible escape towards the caprock and fault.

8 **Conclusion**

This study assessed the extent to which deformation bands could act as efficient mini traps for the geological storage of CO_2. Data from Penrith Sandstone was used to build static geological models and to simulate supercritical CO_2 injection into high-quality reservoirs with low porosity and permeability deformation bands. When considering the role of deformation bands in a CO_2 storage context, it is necessary to evaluate reservoirs in terms of the density of the deformation bands, their location relative to larger structures, the geometry and orientation of the bands, the permeability contrast, the host rock permeability and how these features compartmentalised the reservoir.

Deformation bands can occur as single structures or they can be amalgamated to form cluster zones. Deformation bands within aeolian Penrith Sandstone occur as conjugate sets. In our first attempt, a single conjugate set of deformation bands was considered for the flow simulation. The results demonstrated that although one set of conjugate deformation bands did not compromise the storage capacity, it did improve storage security, based upon their geometry, by structurally trapping the injected CO_2. Deviation of the hinge-line angle from the horizontal could impact the capture and storage of CO_2 by, for example, modifying the spill point.

Deformation bands can extensively influence CO_2 distribution, depending on their permeability when compared to that of the host rock, as the level of permeability contrast would create considerable flow heterogeneities. In some cases, studied herein, the deformation band-host rock permeability contrast was insufficient to act as a reliable mini structural trap. In the context of the structural entrapment of CO_2, the higher contrast scenarios proved more effective.

Deformation bands mainly occur as dense clusters of conjugate sets that mutually cross-cut each other. The sensitivity study performed here was designed to study the effects of deformation band density and geometry; host rock and deformation band permeability contrast; and host rock permeability on CO_2 storage capacity and security. While the resultant plume was uniform and symmetrical in an undeformed case, the plume became progressively distorted as the number of deformation bands increased in the model. Deformation bands will delay the upward migration of CO_2 and reduce reliance on the top seal. The modelling studies suggest that the presence of deformation bands alone may not be a positive contributor to CO_2 storage. Deformation bands need to be abundant, but not overly damage reservoir communication, nor reduce its bulk porosity. They also need to improve sweep efficiency, block the upward movement of CO_2 and more importantly, not cause injectivity issues. The number of deformation bands that were observed at the Penrith Sandstone outcrop, and modelled with three orders of magnitude permeability contrast, did not cause injectivity issues and did contribute to the secure storage of CO_2.

The plume shape lacked radial symmetry and irregularities were exaggerated by increasing permeability disparities. The amount of the free gas reaching the caprock or the leaky fault is not only controlled by permeability variation, but also by the permeability of the host rock, both of which have considerable ramifications for CO_2 storage security.

As deformation bands generally occur in association with normal faults, in one scenario a high transmissibility fault was introduced into a dense cluster of deformation bands. The geometry and the location of the deformation bands against a leaky fault have significant effects on the security of CO_2 storage. Some types of deformation bands demonstrated a more positive contribution to storage security (e.g., deformation bands in conjugate configuration with horizontal intersection angle), while others jeopardised storage security by increasing the amount of free gas that can reach the caprock or leaky fault (e.g., deformation bands perpendicular to the fault).

To improve storage capacity and security it is necessary to consider the optimum injection rate and well placement for the types of reservoirs studied herein. High injection rates may limit storage effectiveness and diminish injection security.

Acknowledgement

AP would like to thank the Centre for Fluid and Complex Systems, Coventry University, UK for providing financial support for this project. The authors also wish to thank Schlumberger for the use of the ECLIPSE and Petrel software and Amarile RE Studio for the use of re-Studio.

AJN, ASB and AEM, published by permission of the Executive Director, British Geological Survey.

References

Antonellini, M. and Aydin, A. (1994) ‘Effect of Faulting on Fluid Flow in Porous Sandstones: Petrophysical Properties’. *AAPG bulletin* 78 (3), 355–377

Antonellini, M., Cilona, A., Tondi, E., and Zambrano, M. (2014a) ‘Fluid Flow Numerical Experiments of Faulted Porous Carbonates, Northwest Sicily (Italy)’. *Marine and Petroleum Geology* [online] 55, 186–201. available from <http://dx.doi.org/10.1016/j.marpetgeo.2013.12.003>

Antonellini, M., Petracchini, L., Billi, A., and Scrocca, D. (2014b) ‘First Reported Occurrence of Deformation Bands in a Platform Limestone, the Jurassic Calcare Massiccio Fm ., Northern Apennines , Italy’. *Tectonophysics* [online] 628, 85–104. available from <http://dx.doi.org/10.1016/j.tecto.2014.04.034>

Arthurton, R.S. and Wadge, A.J. (1981) *Geology of the Country around Penrith: Memoir for 1:50,000 Geological Sheet 24*.

Aydin, A. and Johnson, A.M. (1983) ‘Analysis of Faulting in Porous Sandstones’. *Journal of Structural Geology,* 5 (1), 19–31

Aydin, A. (1978) ‘Small Faults Formed as Deformation Bands in Sandstone’. in *Rock Friction and Earthquake Prediction*. Birkhäuser, Basel, 913–930

Aydin, A., Borja, R.I., and Eichhubl, P. (2006) ‘Geological and Mathematical Framework for Failure Modes in Granular Rock’. *Journal of structural geology* 28 (1), 83–98

Ballas, G., Fossen, H., and Soliva, R. (2015) ‘Factors Controlling Permeability of Cataclastic Deformation Bands and Faults in Porous Sandstone Reservoirs’. *Journal of Structural Geology* [online] 76, 1–21. available from <http://dx.doi.org/10.1016/j.jsg.2015.03.013>

Du Bernard, X., Labaume, P., Darcel, C., Davy, P. and Bour, O. (2002) ‘Cataclastic Slip Band Distribution in Normal Fault Damage Zones, Nubian Sandstones, Suez Rift’. *Journal of Geophysical Research: Solid Earth* 107 (B7), ETG-6

Bernard, X. Du, Eichhubl, P., and Aydin, A. (2002) ‘Dilation Bands: A New Form of Localized Failure in Granular Media’. *Geophysical Research Letters* 29 (24), 1–4

Compton, R.R. (1962) ‘Manual of Field Geology’. *Soil Science* 93 (4), 295

Davis, G.H., Bump, A.P., García, P.E., and Ahlgren, S.G. (2000) ‘Conjugate Riedel Deformation Band Shear Zones’. *Journal of Structural Geology* 22, 169–190

Fachri, M., Rotevatn, A., and Tveranger, J. (2013) ‘Fluid Flow in Relay Zones Revisited: Towards an Improved Representation of Small-Scale Structural Heterogeneities in Flow Models’. *Marine and Petroleum Geology* [online] 46, 144–164. available from <http://dx.doi.org/10.1016/j.marpetgeo.2013.05.016>

Fisher, Q.J. and Knipe, R.J. (2001) ‘The Permeability of Faults within Siliciclastic Petroleum Reservoirs of the North Sea and Norwegian Continental Shelf’. *Marine and Petroleum Geology* 18 (10), 1063–1081

Fossen, H., Schultz, R.A., Shipton, Z.K. and Mair, K. (2007) ‘Deformation Bands in Sandstone:

A Review'. *Journal of the Geological Society* 164 (4), 755–769

Fossen, H., Soliva, R., Ballas, G., Trzaskos, B., Cavalcante, C. and Schultz, R.A. (2017) 'A Review of Deformation Bands in Reservoir Sandstones: Geometries, Mechanisms and Distribution'. *Geological Society, London, Special Publications,* 459 (1), 9–33

Fossen, H., Zuluaga, L.F., Ballas, G., Soliva, R. and Rotevatn, A. (2015) 'Contractional Deformation of Porous Sandstone: Insights from the Aztec Sandstone, SE Nevada, USA'. *Journal of Structural Geology* 74, 172–184

Fossen, H. and Bale, A. (2007) 'Deformation Bands and Their Influence on Fluid Flow'. *AAPG bulletin* 91 (12), 1685–1700

Fowles, J. and Burley, S. (1994) 'Textural and Permeability Characteristics of Faulted, High Porosity Sandstones Textural and Permeability Characteristics of Faulted, High Porosity Sandstones'. *Marine and Petroleum Geology* 11 (5), 608–623.

Gamboa, D., Williams, J.D.O., Bentham, M., Scho, D.I., and Mitchell, A.C. (2019) 'Application of Three-Dimensional Fault Stress Models for Assessment of Fault Stability for CO2 Storage Sites'. *International Journal of Greenhouse Gas Control* 90, 102820

Griffiths, J., Faulkner, D.R., Edwards, A.P. and Worden, R.H. (2018) 'Deformation Band Development as a Function of Intrinsic Host-Rock Properties in Triassic Sherwood Sandstone'. *geological Society, London, Special Publications,* 435 (1), 161–167

Holloway, S., Vincent, C.J., Bentham, M.S., and Kirk, K.L. (2006) 'Top-down and Bottom-up Estimates of CO2 Storage Capacity in the United Kingdom Sector of the Southern North Sea Basin'. *Environmental Geosciences* 13 (2), 71–84

Van Hulten, F.F.N. (2010) 'Geological Factors Effecting Compartmentalization of Rotliegend Gas Fields in the Netherlands'. *Geological Society, London, Special Publications* 1 (347), 301–315

Jamison, W.R. and Stearns, D.W. (1982) 'Tectonic Deformation of Wingate Sandstone, Colorado National Monument.' *AAPG Bulletin* 66 (12), 2584–2608

Leveille, G.P., Knipe, R., More, C., Ellis, D., Dudley, G., Jones, G., Fisher, Q.J. and Allinson, G. (1997) 'Compartmentalization of Rotliegendes Gas Reservoirs by Sealing Faults, Jupiter Fields Area, Southern North Sea'. *London, Special Publications* 123 (1), 87–104

Lewis, C.L.E., Green, P.F., Carter, A., and Hurford, A.J. (1992) 'Elevated K/T Palaeotemperatures throughout Nortwest England: Three Kilometres of Tertiary Erosion?' *Earth and Planetary Science Letters* [online] 112 (1), 131–145. available from <http://www.sciencedirect.com/science/article/pii/0012821X9290012K>

Manzocchi, T., Ringrose, P.S., and Underhill, J.R. (1998) 'Flow through Fault Systems in High-Porosity Sandstones'. *Geological Society, London, Special Publications* 127 (1), 65–82

Matthäi, S.K., Aydin, A., Pollard, D.D. and Roberts, S.G. (1998) 'Numerical Simulation of Departures from Radial Drawdown in a Faulted Sandstone Reservoir with Joints and Deformation Bands'. *Geological Society, London, Special Publications* 147 (1), 157–191

Newell, A.J., Pourmalek, A., Butcher, A.S., and Shariatipour, S.M. (2019) 'The Importance of Lithofacies Control on Fluid Migration in Heterogeneous Aeolian Formations for Geological CO2 Storage: Lessons from Observational Evidence and Modelling of Bleached Palaeoreservoirs at Salt Wash Graben, Utah'. *International Journal of*

Greenhouse Gas Control [online] 91 (December 2018), 1–17. available from <https://doi.org/10.1016/j.ijggc.2019.102841>

Nicol, A., Childs, C., Walsh, J.J., and Schafer, K.W. (2013) 'A Geometric Model for the Formation of Deformation Band Clusters'. *Journal of Structural Geology* [online] 55, 21–33. available from <http://dx.doi.org/10.1016/j.jsg.2013.07.004>

Noy, D.J., Holloway, S., Chadwick, R.A., Williams, J.D.O., Hannis, S.A., and Lahann, R.W. (2012) 'Modelling Large-Scale Carbon Dioxide Injection into the Bunter Sandstone in the UK Southern North Sea'. *International Journal of Greenhouse Gas Control* [online] 9, 220–233. available from <http://dx.doi.org/10.1016/j.ijggc.2012.03.011>

Ogilvie, S.R., Orribo, J.M. and Glover, P.W.J. (2001) 'The Influence of Deformation Bands upon Fluid Flow Using Profile Permeametry and Positron Emission Tomography'. *Geophysical Research Letters* 28 (1), 61–64

Onoja, M.U. and Shariatipour, S.M. (2018) 'The Impact of Gradational Contact at the Reservoir-Seal Interface on Geological CO2 Storage Capacity and Security'. *International Journal of Greenhouse Gas Control* 72 (March), 1–13

Pettijohn, F.J., Potter, P.E. and Siever, R. (1987) 'Introduction and Source Materials'. in *Sand and Sandstone*. Springer, New York, NY, 1–21

Pharaoh, T.C., Morris, J., Long, C.B. and Ryan, P.D. (1996) *The Tectonic Map of Britain, Ireland and Adjacent Areas. Sheet 1: 1 500 000 Scale*.

Qu, D. and Tveranger, J. (2016) 'Incorporation of Deformation Band Fault Damage Zones in Reservoir Models'. *AAPG bulletin* 100 (3), 423–443

Qu, D., Tveranger, J., and Fachri, M. (2017) ‘Influence of Deformation-Band Fault Damage Zone on Reservoir Performance’. *Interpretation* 5 (4), 41–56

Rasband, W.S. (2013) ‘ImageJ v.1.48k (15 December 2013)’. *US National Institutes of Health, Bethesda, Maryland, USA* [online] available from <http://rsb.info.nih.gov/ij>

Rawling, G.C. and Goodwin, L.B. (2003) ‘Cataclasis and Particulate Flow in Faulted, Poorly Lithified Sediment’. *Journal of Structural Geology* 25 (3), 317–331

Ringrose, P. and Bentley, M. (2015) *Reservoir Model Design* [online] Berlin: Springer. available from <http://link.springer.com/10.1007/978-94-007-5497-3>

Romano, C.R., Zahasky, C., Garing, C., Benson, S.M., Shipton, Z.K., and Lunn, R.J. (2020) ‘Subcore Scale Fluid Flow Behavior in a Sandstone with Cataclastic Deformation Dands’. *Water Resources Research* 56 (4), 1–16

Rotevatn, A. and Fossen, H. (2012) ‘Soft Faults with Hard Tips: Magnitude-Order Displacement Gradient Variations Controlled by Strain Softening versus Hardening; Implications for Fault Scaling’. *Journal of the Geological Society* 169 (2), 123–126

Rotevatn, A. and Fossen, H. (2011) ‘Simulating the Effect of Subseismic Fault Tails and Process Zones in a Siliciclastic Reservoir Analogue: Implications for Aquifer Support and Trap Definition’. *Marine and Petroleum Geology* [online] 28 (9), 1648–1662. available from <http://dx.doi.org/10.1016/j.marpetgeo.2011.07.005>

Rotevatn, A., Fossmark, H.S., Bastesen, E., Thorsheim, E., and Torabi, A. (2017) ‘Do Deformation Bands Matter for Flow? Insights from Permeability Measurements and Flow Simulations in Porous Carbonate Rocks’. *Petroleum Geoscience* 23 (1), 104–119

Rotevatn, A., Sandve, T.H., Keilegavlen, E., Kolyukhin, D., and Fossen, H. (2013) ‘Deformation Bands and Their Impact on Fluid Flow in Sandstone Reservoirs: The Role of Natural Thickness Variations’. *Geofluids* 13 (3), 359–371

Rotevatn, A., Torabi, A., Fossen, H., and Braathen, A. (2008) ‘Slipped Deformation Bands: A New Type of Cataclastic Deformation Bands in Western Sinai, Suez Rift, Egypt’. *Journal of Structural Geology* 30 (11), 1317–1331

Rotevatn, A., Tveranger, J., Howell, J.A., and Fossen, H. (2009) ‘Dynamic Investigation of the Effect of a Relay Ramp on Simulated Fluid Flow: Geocellular Modelling of the Delicate Arch Ramp, Utah’. *Petroleum Geoscience,* 15 (1), 45–58

Saillet, E. and Wibberley, C.A.J. (2010) ‘Evolution of Cataclastic Faulting in High-Porosity Sandstone, Bassin Du Sud-Est’. *Journal of Structural Geology* [online] 32 (11), 1590–1608. available from <http://dx.doi.org/10.1016/j.jsg.2010.02.007>

Schmidt, V. and Mcdonald, D.A. (1979a) ‘Texture and Recognition of Secondary Porosity in Sandstones’. *SEPM Special publication* 26, 209–225

Schmidt, V. and Mcdonald, D.A. (1979b) ‘The Role of Secondary Porosity in the Course of Sandstone Diagenesis.’ *SEPM Special publication* 26, 175–207

Schueller, S., Braathen, A., Fossen, H., and Tveranger, J. (2013) ‘Spatial Distribution of Deformation Bands in Damage Zones of Extensional Faults in Porous Sandstones: Statistical Analysis of Field Data’. *Journal of Structural Geology* 52, 148–162

Seers, T.D. and Hodgetts, D. (2016) ‘Extraction of Three-Dimensional Fracture Trace Maps from Calibrated Image Sequences’. *Geosphere* 12 (4), 1323–1340

Shipton, Z.K., Evans, J.P., Robeson, K.R., Forster, C.B. and Snelgrove, S. (2002) 'Structural Heterogeneity and Permeability in Faulted Eolian Sandstone: Implications for Subsurface Modeling of Faults.' *AAPG Bulletin* 86 (5), 863–883

Soliva, R., Schultz, R.A., Ballas, G., Taboada, A., Wibberley, C., Saillet, E., and Benedicto, A. (2013) 'A Model of Strain Localization in Porous Sandstone as a Function of Tectonic Setting, Burial and Material Properties; New Insight from Provence (Southern France)'. *Journal of Structural Geology* [online] 49, 50–63. available from <http://dx.doi.org/10.1016/j.jsg.2012.11.011>

Sternlof, K.R., Pollard, D.D., and Durlofsky, L.J. (2006) 'Flow and Transport Effects of Compaction Bands in Sandstone at Scales Relevant to Aquifer and Reservoir Management'. *Water Resources Research* 42, 1–16

Stow, D.A. V (2005) *Sedimentary Rocks in the Field*. Gulf Professional Publishing

Tondi, E., Antonellini, M., Aydin, A., Marchegiani, L., and Cello, G. (2006) 'The Role of Deformation Bands, Stylolites and Sheared Stylolites in Fault Development in Carbonate Grainstones of Majella Mountain, Italy'. *Journal of Structural Geology* 28 (3), 376–391

Torabi, A. and Fossen, H. (2009) 'Spatial Variation of Microstructure and Petrophysical Properties along Deformation Bands in Reservoir Sandstones'. *AAPG bulletin* 93 (7), 919–938

Torabi, A., Fossen, H., and Alaei, B. (2008) 'Application of Spatial Correlation Functions in Permeability Estimation of Deformation Bands in Porous Rocks'. *Journal of Geophysical Research: Solid Earth* 113 (February), 1–10

Torabi, A., Fossen, H., and Braathen, A. (2013) 'Insight into Petrophysical Properties of Deformed Sandstone Reservoirs'. *AAPG bulletin* 97 (4), 619–637

Turner, P., Burley, S.D., Rey, D., and Prosser, J. (1995) 'Burial History of the Penrith Sandstone (Lower Permian) Deduced from the Combined Study of Fluid Inclusion and Palaeomagnetic Data'. *Geological Society, London, Special Publications* 98 (1), 43–78

Twiss, R.J and Moores, E.M. (1992) *Structural Geology*. Macmillan

Underhill, J.R. and Woodcock, N.H. (1987) 'Faulting Mechanisms in High-Porosity Sandstones; New Red Sandstone, Arran, Scotland'. *Geological Society Special Publication* 29 (1), 91–105

Walsh, J.J. and Heath, A.E. (1998) 'Assessment of the Effects of Sub-Seismic Faults on Bulk Permeabilities of Reservoir Sequences'. *Geological Society, London, Special Publications* 127 (1), 99–114

Zuluaga, L.F., Rotevatn, A., Keilegavlen, E., and Fossen, H. (2016) 'The Effect of Deformation Bands on Simulated Fluid Flow within Fault-Propagation Fold Trap Types: Lessons from the San Rafael Monocline, Utah'. *AAPG bulletin* 100 (10), 1523–1540